T-4149

AN ANALYSIS OF THE PROCESS-INDUCED PIPING DEFECT IN EXTRUSION WITH CONICAL DIES

by

Gokhan Erdem

T-4149

A thesis submitted to the Faculty and the Board of Trustees of the Colorado School of Mines in partial fulfillment of the requirements for the degree of Master of Science (Metallurgical and Materials Engineering).

Golden, Colorado
Date: Dec. 3, 1991

Signed: Gokhan Erdem
Gokhan Erdem

Approved: Cheatle J Van Tyne
Dr. C.J. Van Tyne
Thesis Advisor

Golden, Colorado
Date: Dec. 3, 1991

Dr. John J. Moore
Professor and Department Head, Department of Metallurgical and Materials Engineering

ABSTRACT

The piping defect which can occur near the end of the stroke in the extrusion process with conical dies has been modeled by applying the upper bound approach and the finite element method. The influence of the process conditions such as billet length, die angle, radius, and reduction ratio on the formation of piping defect is presented.

For the extrusion process both with and without a pipe, kinematically admissible velocity patterns have been developed and analyzed by the upper bound approach. The analyses divide the workpiece into four zones separated by three surfaces of velocity discontinuity. The power terms are calculated for each zone separately and the formation of the piping defect is investigated. The results which were obtained from the upper bound method were used to determine criteria for the occurrence of the piping defect as a function of the major process parameters. It is observed that decreasing the billet length, increasing the die angle, increasing the product radius and increasing the non-angled portion of the die cause an increased potential for formation of the piping defect. Although the friction causes a large increase in the required extrusion pressure,

an increase in the friction factor increases the domain for piping by a small amount.

The extrusion process is also analyzed by the finite element method (FEM). The results obtained from the upper bound approach have been correlated to the results from the finite element method. The finite element method exhibits reasonable agreement with the upper bound model for both the prediction of pipe size and the criteria curve for the prevention of the piping defect.

TABLE OF CONTENTS

LIST OF FIGURES

LIST OF TABLES

NOMENCLATURE

A	=	dimensionless function
B	=	dimensionless function
e	=	dimensionless function
E	=	Young's modulus
f	=	dimensionless function
J^*	=	upper bound on power
k	=	Mises' yield constant
L	=	length of the non extruded portion of the billet
m	=	constant friction factor
p	=	dimensionless function
p_{AVE}	=	average ram pressure
q	=	dimensionless function
R	=	cylindrical coordinate in radial direction
R_a	=	radius of the angled portion of the die
R_i	=	product radius
R_o	=	ram radius
S	=	surface
S_{Ti}	=	surface of velocity discontinuity
t	=	time
T_i	=	external traction

$\dot{U}$ = velocity of ram

$\dot{U}_R$ = radial component of velocity

$\dot{U}_y$ = axial component of velocity

$\dot{U}_\theta$ = circumferential component of velocity

v_i = velocity

V = volume

V_{II} = slope of W(R) as a function of R

V_{III} = slope of Z(R) as a function of R

Δv = tangential velocity difference

$W(R)$ = axial position of die face as a function of R

$\dot{W}_i$ = internal power of deformation

$\dot{W}_s$ = shear power losses

$\dot{W}_f$ = frictional power losses

y = cylindrical coordinate in axial direction

$Z(R)$ = axial position of Γ_3 surface as a function of R

α = conical die angle

β = dimensionless function

γ = dimensionless function

δ = crack length (a pseudo-independent parameter)

ε = position of Γ_3 surface on axis of symmetry (a pseudo-independent parameter)

$\dot{\varepsilon}_{ij}$ = strain rate

ρ = dimensionless radial position variable

σ_o = yield strength in uniaxial tension

θ = cylindrical coordinate in circumferential direction

τ = shear stress

ACKNOWLEDGEMENT

I am very thankful to Dr. Chester J. Van Tyne, my thesis advisor, for his guidance, patience, valuable discussions, and helpful comments during my research at Colorado School of Mines.

It is a pleasure to express my deep gratitude to Dr. George Krauss and Dr. Robert H. Frost for serving as members on the committee and their assistance to this study.

For financial support throughout this research, I would like to thank Eregli Iron and Steel Inc. Partial support of a portion of this work by the AMAX Foundation is gratefully acknowledged.

Special thanks are due to Mr. W.A. Gordon of Torrington Company for interest in my research.

Finally, I owe a considerable debt to my family who provided help and understanding in a great number of ways. Especially, I would like to thank to my grandmother Hayriye Tetik, my father Abdurrahman Erdem and my mother Ozden Erdem for their love and support.

1. INTRODUCTION

Metal deformation processes can be viewed as systems with a large number of interacting variables such as material properties of the workpiece and the tooling, tribological conditions in the contact zone between the work piece and tools, the tool geometry, process temperature, velocity, etc. In metal forming, the prediction of metal flow is a very important consideration under a given set of processing conditions. Thus, many metal forming models require a good understanding of the interaction between these parameters in order to operate actual processes with optimal metal flow.

The modeling of metal forming processes can be considered as a key to improved product quality and optimized production. The primary reason for using a model is that it can yield information about the actual process, which would be inaccessible or expensive to provide without the model (1). The other aim of a model is the generation of quantitative statements concerning the process parameters. This quantification can be used to determine the optimal manufacturing conditions for a forging or extrusion. The results generated by the model should be more readily accessible, less costly or more complete than can be

obtained by laboratory experiments or tests during actual manufacturing. Clearly, the need for the development of process models is particularly great in situations where it is technically difficult to measure the process parameters in question. When complicated die geometry, complex material characteristics, including work hardening, tribological conditions, etc. are considered, mathematically exact solutions for the actual metal forming become very difficult, if not impossible.

Many idealized models (1-5) are usually assumed to find approximate solutions to real metal forming problems. Among the various approximation methods for solution, limit analysis (3,4) is an analytical approach often used for metal forming operations. Two separate solutions are developed: one is the upper bound solution, which provides a value for the required power that is equal or greater than the actual power and the other one is the lower bound solution, which provides a value that is equal or lower than actual power. Hence, the actual value is bracketed between the two limits.

When applying the upper bound approach, the first step of the investigation is to assume a velocity field for the deforming body. Velocity can be measured directly or it can sometimes be observed in model experiments. For a lower

bound solution, however, the first step is the formulation of a stress tensor, which is far more difficult to conceive and can be measured only indirectly from experimentation. Therefore, the upper bound approach is used more often for theoretical analysis of metal forming processes.

The upper bound method considers kinematically admissible velocity fields (i.e. those which satisfy the incompressibility requirement and the velocity boundary conditions). From the velocity field the internal power of deformation, the internal shear power losses and the frictional power losses are computed and summed to determine the total power required for deformation. From the knowledge of the total forming power and the tooling geometry and velocity, the instantaneous forming load or averaged forming pressure can be determined.

An upper bound solution can provide information about the effect each individual process parameter has on the loads required for the actual manufacturing process. More important, the upper bound method coupled with principle of minimum energy can be used to indicate process conditions which might produce a defect during metal forming operations (4,7-9). A piping defect, which can occur during forging or extrusions, is produced because the flow associated with such defect formation is energetically more favorable under

the given process conditions than sound flow. The prediction of piping defect is a matter of establishing under what conditions the energy for defect formation is less than that for sound flow.

The work presented in this study analyzes the piping defect in extrusions. Figure 1 shows the formation and growth of an actual piping defect in lead (10). The formation of the piping defect is not desirable. A considerable portion of the material can be rendered useless in the extruded product because of it. Knowledge of the processing conditions which cause this type defect will aid the design engineer considerably, by providing reliable information about the non-defect processing requirements without expensive, time-consuming laboratory and plant-scale experiments.

In addition to the piping defect in extrusions, a similar type of defect can occur in forgings due to the material flow away from a die face (see Figure 2). This type of flow produces a cavity similar to a pipe and it is known in the forging industry as the extrusion defect (11). The results from the present work on extrusion can be judiciously applied to forging processes so that this type of defect can be avoided.

The axisymmetric process examined in this work is

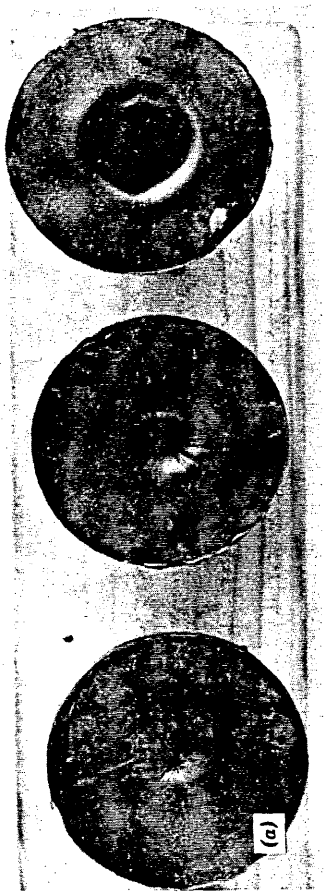

Figure 1 The sequential formation and growth of a piping defect in lead (10).

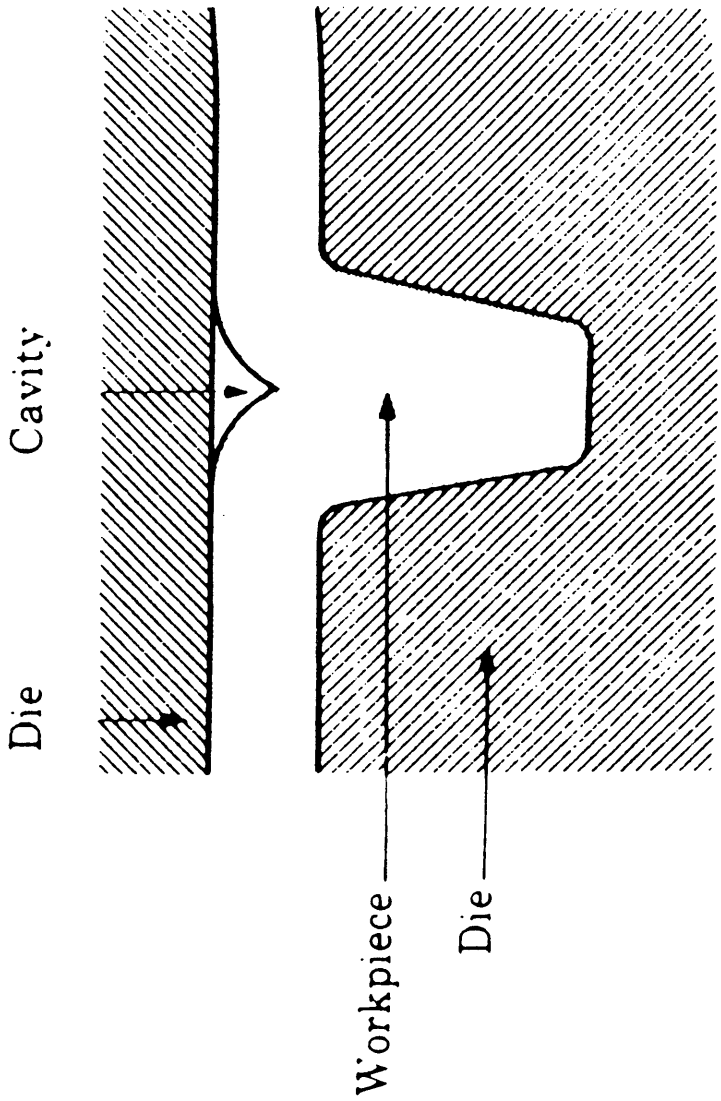

Figure 2 Defect in forging due to material flow pattern into the die cavity (11).

schematically shown in Figure 3. The initial billet is a cylinder of radius R_o. The billet is in contact with the chamber wall. The length of this contact is L which is also the length of the non extruded portion of the billet. In the extrusion process understudy, the ram pushes on the back side of the billet with a velocity $\dot{U}$. A rod of radius R_i exits the extrusion die with a velocity v_f.

Figure 4 shows the criteria developed by Avitzur. The critical relative length when piping begins for three constant friction factor, m, can be seen. Figure 5 illustrates the criteria for the start of the piping defect developed by Gordon and Van Tyne.

Near the end of the stroke in a extrusion process, a cavity can be produced at the back end of the billet. The billet material along the axis of symmetry is moving forward more rapidly than the ram and a separation occurs (see Figure 6). This cavity is termed a pipe since the product is a tube or a pipe rather than a solid rod. When the piping cavity starts the extrusion process should be stopped so that no defective product is produced (8).

There have been several analyses of the piping defect by other investigators. Johnson established a very simple criteria for the piping defect in a plane strain extrusion process (12,13). He indicates that a pipe will form when

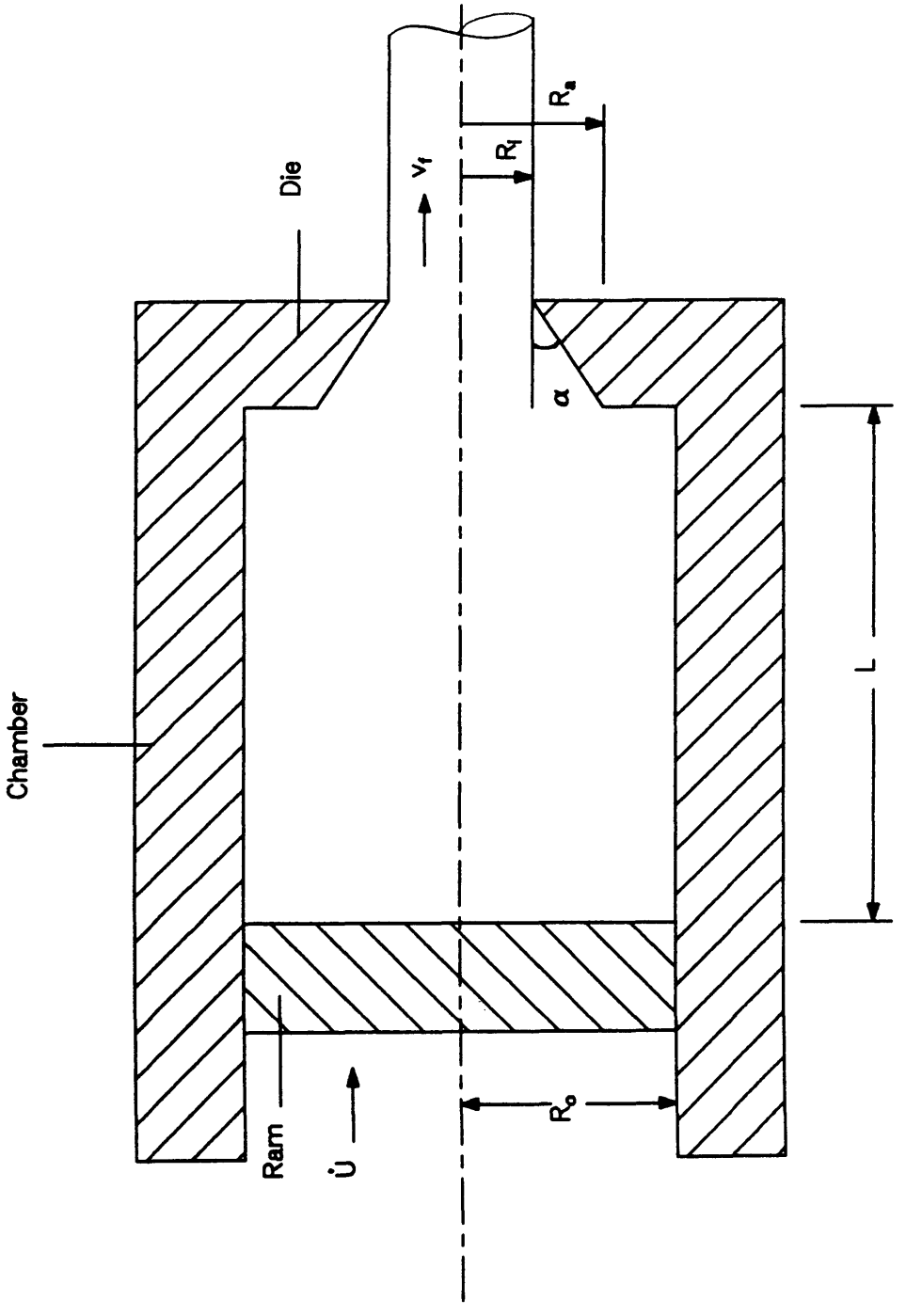

Figure 3 Schematic of the extrusion process, with the tooling, geometrical variables and velocities shown.

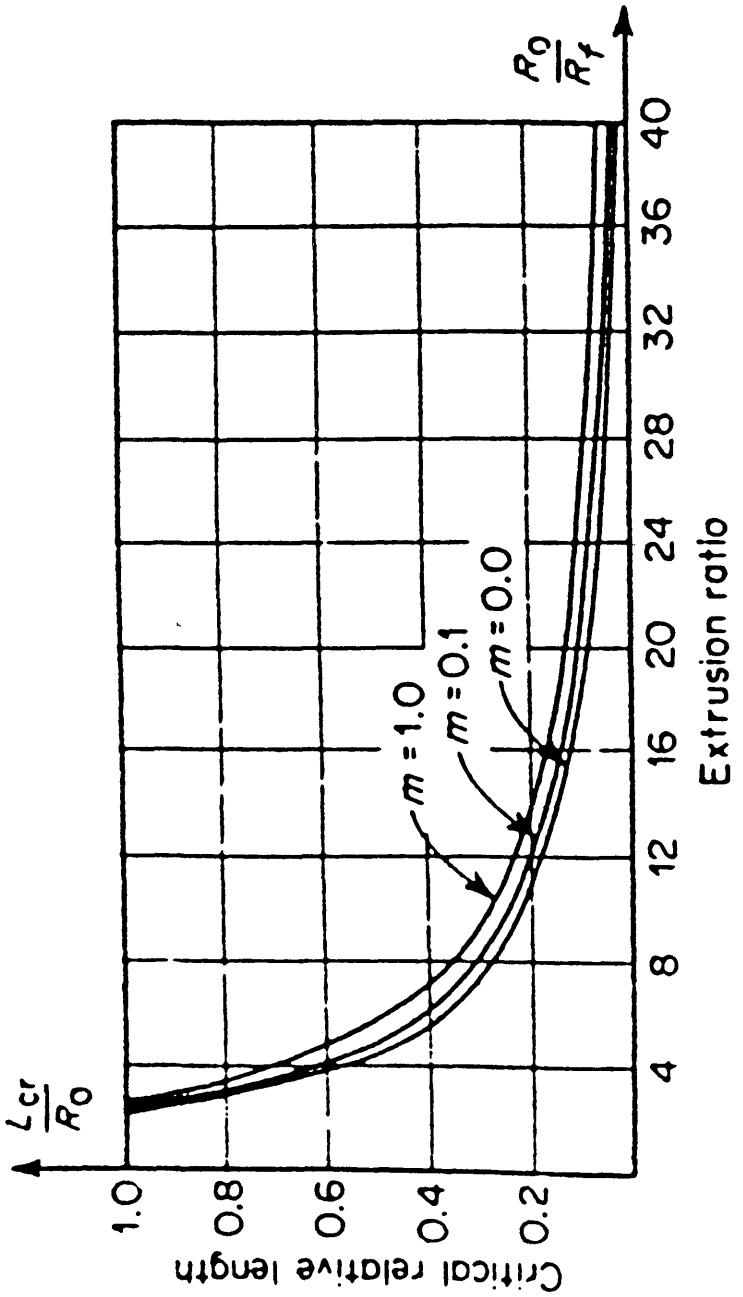

Figure 4 Critical relative length at which piping begins (3).

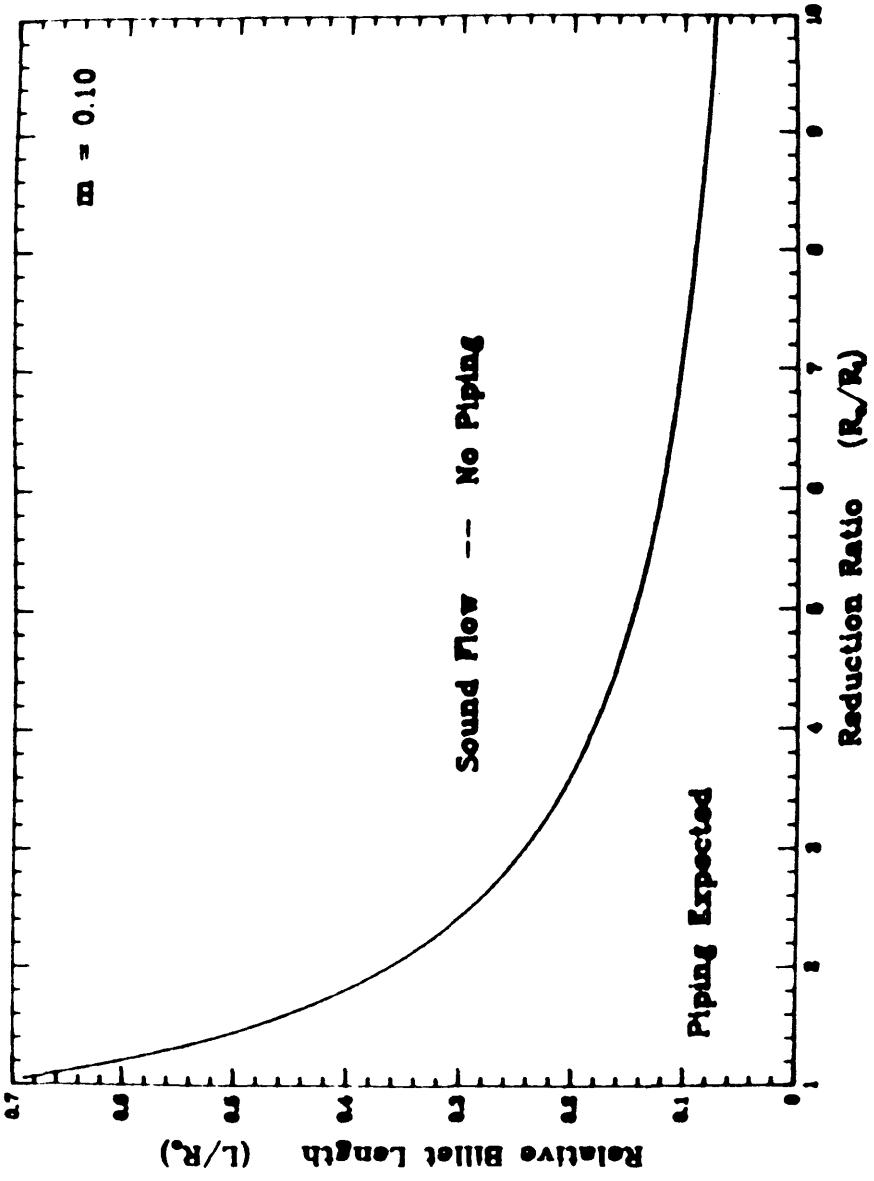

Figure 5 Criteria for the start of the piping defect (8).

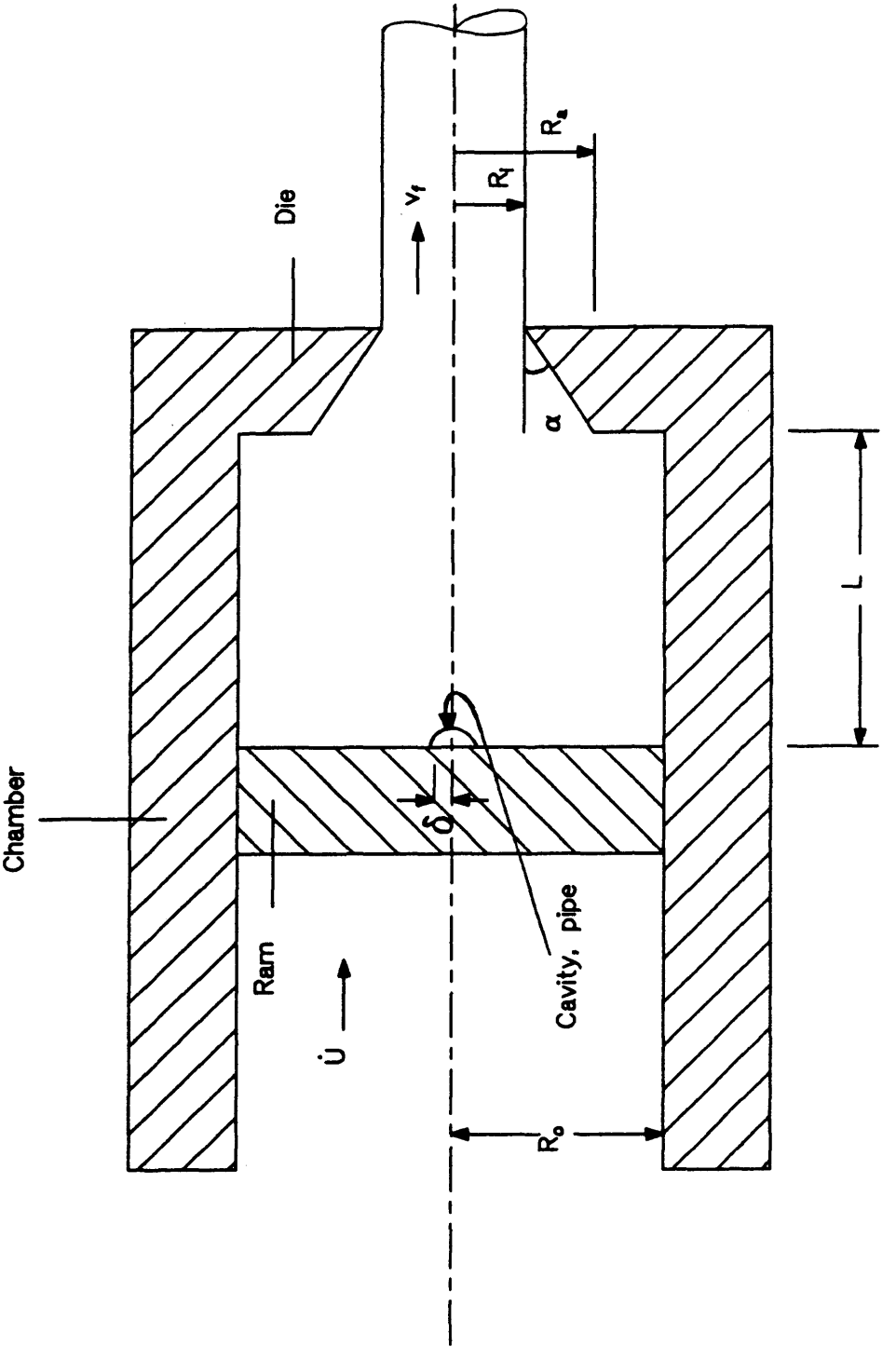

Figure 6 Schematic of the extrusion process near the end of the stroke showing the formation of a pipe with radius δ.

the product width is larger than one half the length of the non extruded part of the billet. In the present analysis this would be equilavent to $R_i > L$. Avitzur (3) has used the upper bound approach to analyze the piping defect. His analysis uses a two zone velocity field. The die has a conical region of angle α and radius R_a. A three zone velocity field has been used by Gordon and Van Tyne (8) to examine the piping defect at the end of the stroke in extrusions with flat dies (i.e. $\alpha = 90°$). This study uses a four zone velocity field and the upper bound approach to examine the formation of a pipe in an extrusion with a conical die.

This study uses another powerful mathematical technique called the finite element method (FEM) to examine the formation of pipe. The FEM program utilized in this work is NIKE2D which is an implicit finite deformation formulation developed by J.O. Hallquist at the Lawrence Livermore National Laboratory (14). NIKE2D uses the interactive preprocessor program called MAZE and the interactive post-processor called ORION (15-16). The primary focus of an FEM analysis for plastic deformation is on the internal stress and strain states that the workpiece experiences during the forming operation. The upper bound approach which is based on energy balance technique cannot provide these stress and

strain states. The most notable disadvantage of the finite element analysis are the inaccuracy of the derivatives of the approximated solution, the difficulty in imposing the boundary conditions along nonstraight boundaries, the difficulty in accurately representing geometrically complex domains, and the inability to employ nonuniform and nonrectangular meshes (17). In this study the reason for the FEM analysis is primarily to confirm the results which are determined from the upper bound method.

2. BACKGROUND

2.1 THE UPPER BOUND APPROACH

In general, because of the complexity of the mathematics, exact analytical solutions for metal forming processes and operations are extremely difficult, and, at present approximations and simplifying assumptions are inevitable. Analytical models rely on the closed-form solution of the plasticity equations to obtain information about forming loads, tool-workpiece interface pressure distributions, etc. These methods are typically applicable only for the simplest of geometries and boundary conditions (18). There are several requirements for exact analytical solutions and they can be obtained only by following strict rules to satisfy completely a predetermined set of conditions (3-5). The requirements:

1. The equations of equilibrium for the stress tensor must be satisfied throughout the deforming body.
2. Continuity of flow must be maintained; that is, volume constancy must be satisfied.
3. The relationship between internal stresses and flow in the real material must be known and obeyed.
4. The geometric and static boundary conditions must be satisfied, including friction behavior over the indent

interface between the tool and the workpiece.

When all of the above conditions are satisfied, the solution completely and uniquely determines the state of the stress and the state of strain throughout the entire workpiece and over its boundaries. Because of the complexity of these restrictions and the nature of the equations, there is no set prescription for obtaining a complete solution. In fact, there is not presently available one complete solution for the unique stress and strain fields in the workpiece of any metal-forming process. However, when an upper bound solution is developed, some of the exact conditions are satisfied, while others are relaxed (3-5). By relaxing several of the necessary conditions, the upper bound solution loses its uniqueness. For an upper bound solution, the requirements are relaxed to the extent that the equations of equilibrium, the stress-strain relationship, and the stress-boundary conditions are not necessarily satisfied. An infinite number of flow patterns can satisfy the relaxed conditions for an upper bound solution. The actual solution will be one which provides the lowest upper bound.

The upper bound approach often uses a simplified version of material behavior. Although this is not totally realistic, it does reasonablely approximate the material

properties of metals which are being hot worked. If this simplification were not used, then the equations used by the upper bound would be too complex to be solved mathematically negating the possibility of a solution being determined. The workpiece material is also assumed to be homogenous and isotropic. Therefore, the effects of strain hardening, strain rate hardening and/or strain induced softening on the flow stress are ignored. The deviatoric stress tensor for a Mises material is related to the strain rate tensor in such a manner that if all strain rate components are changed proportionately, the deviatoric stress components remain unchanged (3-5).

A description of the upper bound approach as an application of limit analysis to metal forming processes is presented by Avitzur (4). The upper bound theorem formulated by Prager and Hodge (19) states that of all kinematically admissible strain rate fields, the one that occurs, minimizes the expression:

$$J^* = \sqrt{2}\, k \int_v \sqrt{\dot{\varepsilon}_{ij}\, \dot{\varepsilon}_{ij}}\, dV - \int_{s_t} T_i\, v_i\, dS \qquad (1)$$

where J^* is the upper bound on power,

k is the shear yield strength of the material,

ε_{ij} is a strain rate component,

V is the volume of the deforming material,

T_i is an external traction,

v_i is a velocity component, and

S_t is the surface over which the traction is exerted.

In this approach, since the material is assumed to be a perfectly plastic material, which obeys the Mises stress-strain rate relation, (i.e. no volumetric change and no work-hardening), the relationship between the shear yield strength and the flow strength of the material, σ_o, is

$$k = \frac{\sigma_o}{\sqrt{3}} \tag{2}$$

When Eq. (2) is substituted into Eq. (1), the upper bound equation becomes:

$$J^* = \frac{2\sigma_o}{\sqrt{3}} \int_v \sqrt{\frac{1}{2}\, \dot{\varepsilon}_{ij}\, \dot{\varepsilon}_{ij}}\, dV - \int_{s_t} T_i\, v_i\, dS \qquad (3)$$

The first term on the right side of Eq. (3) is the internal power of deformation, and the second term is the power required to overcome external tractions, T_i, opposing the deformation process.

In metal forming operations, shear power along surfaces of velocity discontinuity within the deforming workpiece and frictional power loses between the tool and the workpiece need to be included. These additions presented by Drucker (20), modify Eq. (3) to become:

$$J^* = \frac{2\sigma_o}{\sqrt{3}} \int_v \sqrt{\frac{1}{2}\, \dot{\varepsilon}_{ij}\, \dot{\varepsilon}_{ij}}\, dV + \int_{s_{\Gamma_1}} \tau_s |\Delta v|\, dS + \int_{s_{\Gamma_2}} \tau_f |\Delta V|\, dS - \int_{s_t} T_i\, v_i dS \qquad (4)$$

where τ_s is the internal shear stress,

τ_f is the frictional stress on the interface,

$S_{\Gamma 1}$ is a surface of velocity discontinuity within

the deforming workpiece, and

S_{r2} is a surface between the tool and the workpiece where friction is present.

This form of the equation has been used extensively for upper bound solutions of metal forming processes. The first term on the left side of Eq. (4) represents the power for internal deformation over the volume of the deforming body. The second term includes all the shear power losses over internal surfaces of velocity discontinuity. The third term includes the power losses due to friction between the tooling and the workpiece and the last term is the power supplied to overcome any external tractions.

In the upper bound approach, because the body is fully plastic, the friction is usually described by the constant friction factor formulation. This relationship is assumed to occur at all workpiece-tool interfaces. Therefore, the friction stress is

$$\tau_f = \frac{m\,\sigma_o}{\sqrt{3}} \qquad (5)$$

where m is the constant friction factor.

This friction factor 'm' is assumed constant for a given

die, workpiece, and lubricant under constant surface and temperature conditions (3-6,21). It has values between 0.0 for frictionless conditions and 1.0 for sticking friction.

In order to analyze a metal flow process by applying the upper bound analysis, it is necessary to make several assumptions and to perform the following steps (3-6).

1. Assume a velocity field which satisfies the conditions of incompressibility and the velocity boundary conditions.
2. Calculate the energy rates for deformation such as the internal power of deformation, the frictional power losses, the internal shear power losses etc.
3. Determine the total energy, J^*.
4. Assume another velocity field and find if it produces a lower J^*.

This process continues until the lowest J^* is determined.

The deformation load for the process can be obtained by dividing the energy rate by the normal velocity of the die acting on the workpiece. The total energy rate, J^*, can be expressed as

$$J^* = \dot{W}_{internal} + \dot{W}_{shear} + \dot{W}_{friction} \quad (6)$$

$$= \text{Load x Die Velocity}$$

By the upper bound theorem (3-4), the load calculated will be greater than the actual load and hence represent an upper bound to the actual forming load. When the upper bound load becomes lower, the prediction becomes better.

In order to examine a large number of flow patterns at the same time, the velocity field may contain an extra parameter. This parameter is often used to determine the position of one of the internal surfaces of velocity discontinuity. The value of this parameter, which minimizes the total power of deformation, is the one that provides the most realistic velocity field. This parameter can also be used to determine whether or not a defect would exist under a given set of process conditions. Although this parameter is initially considered as an independent variable, it is not truly independent since its value is determined by minimizing the total power. Because of the dual characteristic of independency and dependency, this variable is classified as a pseudo-independent parameter.

Often, the flow pattern for deformation processes includes one or more pseudo-independent parameters (4) whose values are determined by minimizing the total energy rate, J^*, with respect to such parameters. When the number of pseudo-independent parameters increases in the flow pattern, the solution improves, but the mathematical computations

become more complex. More detailed information about the use of a pseudo-independent parameter for the determination of the pipe defect in extrusions is given in Section 4.

2.2. THE FINITE ELEMENT METHOD IN METAL FORMING PROCESS MODELING

Process modeling for deformation mechanics has been a major concern in metal working technology. Proper design and control of metal forming processes requires global as well as local knowledge of the mechanics during deformation. Several analytical techniques are available which simulate the forming of metals. As computers become increasingly efficient, the numerical modeling of metal forming processes is an attractive and economical means of understanding a variety of metal working operation (22).

The finite element method (FEM) is a powerful technique for determining stresses and displacements in deforming workpiece too complex for strictly analytical methods. Indeed the finite element process is established as a general numerical method for solutions of partial differential equation systems, subject to known boundary and/or initial conditions (17). This method has found greater usage in engineering practice due to the common use of computer graphics and availability of powerful computer workstations. The finite element method appeared in the metal forming field in the early 1970s. When this method was introduced for the analyses of metal forming processes, accurate determination of the effects of various parameters

involved in the processes in the detailed metal flow became possible (23). The first applications of the finite element analysis utilized infinitesimal elasto-plastic formulations for small deformations (24,25) and soon it became evident that metal forming required greater sophistication.

In order to simulate metal flow during a deformation process by the finite element method, a number of finite points are identified in the domain of the workpiece. These points are called nodal points. The domain of the function being sought is represented approximately by a finite collection of subdomains called finite elements. The domain then is composed of an assemblage of elements connected together appropriately within each element by continuous functions which are uniquely described in terms of the nodal point values associated with the particular element. The basis of finite element metal flow modeling, using the variational approach, is to formulate proper functionals, depending upon specific constitutive relations. The solution of the original boundary value problem is obtained by the solution of dual variational problem where the first-order variation of the functional vanishes. An approximate interpolation function for the field variable is used within these elements. The functional is expressed locally within each element in terms of the nodal points. The local

element equations are then assembled into the overall problem. Thus, the functional is approximated by a function of global nodal point values (23).

In many metal forming operations, the geometry of the workpiece changes with time. Part of the surface that was free may come in contact with the tooling, becoming restricted in the normal direction with frictional forces applied in the tangential direction. The possibility of defining one or more dies, moving or not, with arbitrary shape, together with all geometric verifications and adoptions, requires sophisticated programming. These procedures can be done by commercial finite element programs which have pre- and post-processors (26).

The advancements in the application of the finite element method have been mainly toward expanding its applicability to a variety of metal forming processes. With continual effort on improving the finite element technique, this method has became a most powerful theoretical tool in analyzing metal forming problems. Recently, the finite element method has been used to calculate parameters that change locally with deformation, such as, the parameters used in damage rules (27,28). Almost all FEM applications so far have dealt with two dimensional problems, but this method will undoubtedly be extended to three-dimensional

problems.

3. OBJECTIVE OF STUDY

The axisymmetric extrusion process examined in this investigation is used to produce a cylindrical rod. This study models the process by dividing the workpiece into four deformation regions. Both sound flow and defect flow patterns are analyzed. The criteria for the occurrence of the piping defect as a function of the process parameters for extrusion through conical dies is developed based on an upper bound approach. The criteria separate regions of sound flow from regions where piping would most likely occur.

The reason for using the upper bound approach is that there is no available method for finding exact analytical solutions in metal forming operations, and more importantly, the upper bound approach coupled with the principle of minimum energy can be used to indicate the conditions when piping would occur.

The goal of the present study is to determine the process parameters such as billet geometry, tooling design, and friction conditions which induce a pipe. This knowledge will provide a means of understanding the process and allows the optimal manufacturing conditions without the cost and time involved with the traditional trial and time error investigation.

In addition to the upper bound approach, the finite element method is applied to the extrusion process. The relative pipe size and the first appearance of a pipe are determined by the finite element method. The finite element method results are used to verify the results obtained from the upper bound method.

4. ANALYSIS OF THE PROCESS

4.1 UPPER BOUND ANALYSIS

The process to be analyzed is shown in Figures 3 and 6. The cylindrical coordinate system (R,θ,y) is assumed to have the y axis along the axis of symmetry and the origin is fixed to the left end of the billet. The billet is assumed to be a Mises material with a flow stress σ_o. The initial cylindrical billet begins with a radius R_o. The non extruded portion of the billet has a length L. The ram pushes on the back side of the billet with a velocity $\dot{U}$. The cylindrical product exits the extrusion die with a velocity v_f. The radius of the product is R_i. The extrusion die has a conical region of radius R_a and angle α.

A schematic representation of one half of the process is given in Figure 7. The workpiece is divided into four zones. Zone I is the outer portion of the billet and it is a ring element of inner radius R_a, outer radius R_o and thickness L. The side of zone I adjacent to the rams moves in the same direction as the ram with velocity $\dot{U}$. Zone IV is the product and it is assumed to be rigid body which moves with a velocity v_f. Zone III is a complex-shaped region in which both axial and radial flow are occurring. Material deformation is occurring in zone III. Zone II is

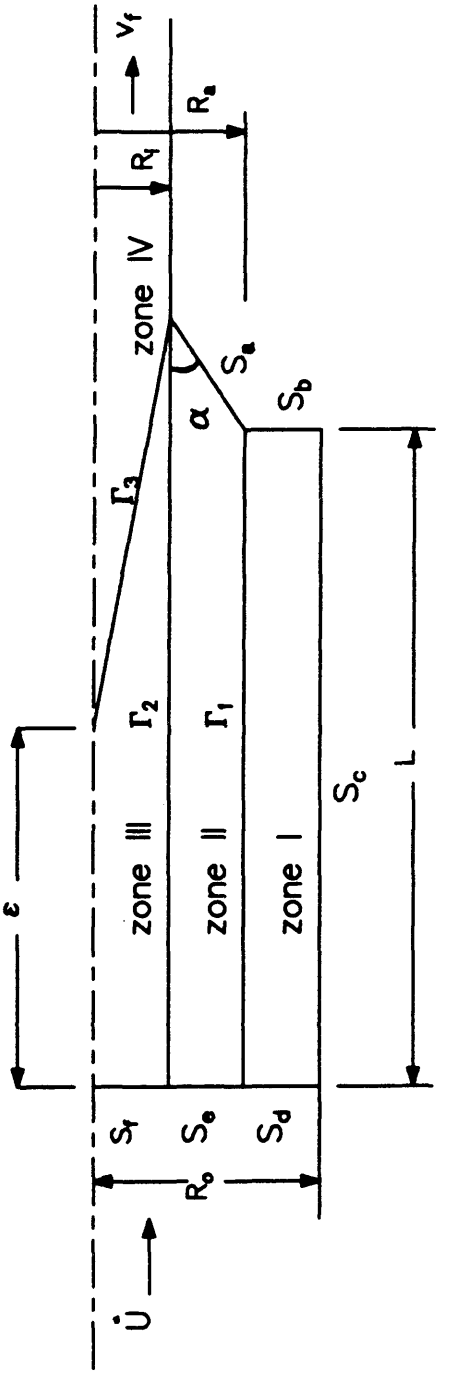

Figure 7 Schematic representation of the sound flow velocity field for the lower half of the workpiece being extruded.

similar to zone III and there is also material deformation in this zone. The volumes of zone II, zone III and zone IV are all dependent on the die angle α and a pseudo-independent parameter, ε, whose value changes with the other process variables. In order to use the upper bound approach, the velocity fields must be determined for each zone.

As seen in Figure 7, S_a is the interfacial surface between zone II and the die. S_b is the interfacial surface between zone I and the die. S_c is the interfacial surface between zone I and the chamber. S_d is the interfacial surface between zone I and the ram. S_e is the interfacial surface between zone II and the ram. S_f is the interfacial surface between zone III and the ram.

The four zones are separated by three surfaces of velocity discontinuity. Surface Γ_1 is a cylindrical surface which separates zone I from zone II. The surface is fixed at the radial position R_a. Surface Γ_2, which separates zone II and zone III, is also a cylindrical surface, bit at the radial position R_i. The surface Γ_3, which is assumed to be a conical surface, between zone III and zone IV is shown as a linear function in Figure 7. Its exact position is variable, depending on the pseudo-independent parameter ε. The actual value that ε possesses is determined through the

principle of minimum energy. Under the processing conditions that cause a positive optimal value for ε, the material will be deformed to produce a sound flow. If the optimal value of ε is negative, then separation between the billet and the ram will occur. A schematic representation of this case is shown in Figure 8. When the billet material along the axis of symmetry moves forward more rapidly than the ram, a cavity occurs which is termed a pipe since the product is a tube or a pipe. Therefore, the value of ε can be used to determined whether or not, for a set of geometric and process conditions, piping would occur. If the piping cavity were present the radius of the pipe would be given by the value δ as illustrated in Figure 8.

The axial location of the Γ_3 surface can be expressed as a function of the radial component, R. If Z is the axial position of Γ_3, then for $\varepsilon > 0$, the relative axial position is given by

$$\frac{Z}{R_i} = \left(\frac{L}{R_o}\frac{R_o}{R_i} - \frac{\varepsilon}{R_i}\right)\rho + \frac{\varepsilon}{R_i} \qquad (7)$$

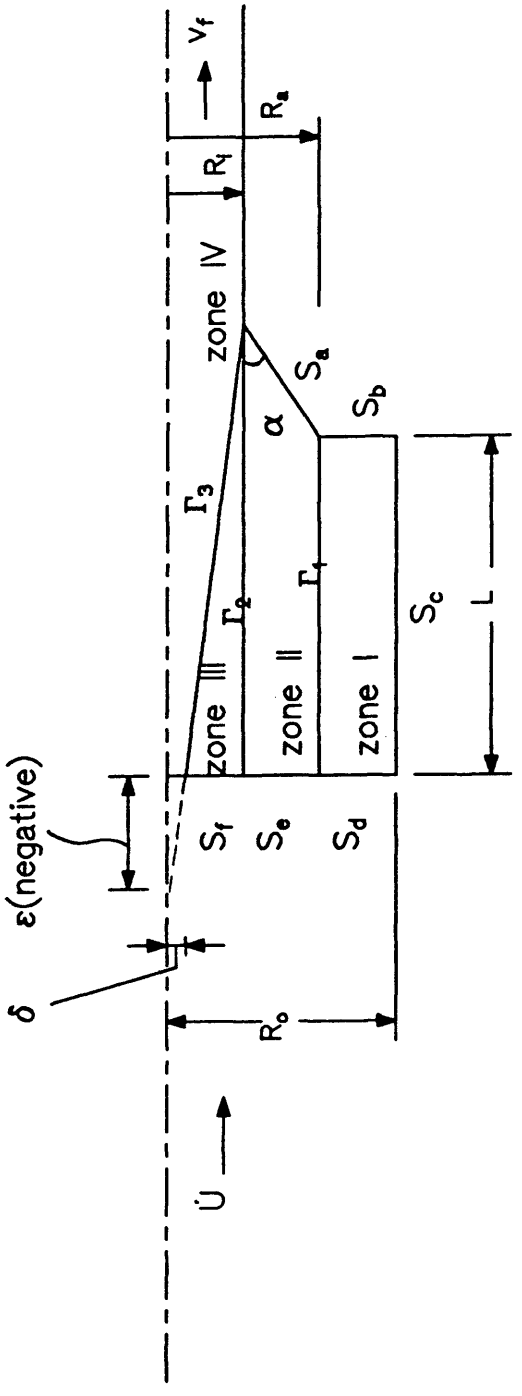

Figure 8 Schematic representation of the defect flow velocity for the lower half of the workpiece being extruded with a pipe of radius δ.

where

$$\rho = \frac{R}{R_i} \tag{8}$$

For any constant value of θ, this is an equation of straight line, which is to be expected since Γ_3 is a conical surface.

If $\varepsilon < 0$, then the axial position of Γ_3 as a function of R can be expressed in terms of δ. In this case

$$\frac{Z}{R_i} = \frac{L}{R_o}\frac{R_o}{R_i}\frac{\rho - \frac{\delta}{R_i}}{1 - \frac{\delta}{R_i}} \tag{9}$$

The values of ε and δ are also related to one another. Such a relationship is shown graphically in Figure 8. This relationship can be expressed mathematically by using the point where $\rho = 0$. At this point $Z = \varepsilon$ and substituting into Eq. (9), one obtains

$$\frac{\varepsilon}{R_i} = \frac{L}{R_o}\frac{R_o}{R_i}\frac{-\frac{\delta}{R_i}}{1-\frac{\delta}{R_i}} \tag{10}$$

In order to obtain δ as a function of ε, Eq. (10) can be rearranged, yielding

$$\frac{\delta}{R_i} = \frac{\frac{\varepsilon}{R_i}}{\frac{\varepsilon}{R_i} - \frac{L}{R_o}\frac{R_o}{R_i}} \tag{11}$$

The derivations of the velocity fields and the power terms for each zone are presented in Appendix I. A summary of this work is presented below. The equations for defect flow using the pseudo-independent parameter δ will be presented below. The equivalent equations for sound flow using ε can be obtained by substitution of Eq. (11) in the equations that follow. The final equation for the ram pressure is a function of process geometry, frictional conditions and the pseudo-independent parameter.

The velocity field for each zone is calculated in cylindrical coordinates. The velocity field for each zone

is as follow:

For zone I

$$\begin{aligned} \dot{U}_R &= -\frac{\dot{U}R}{2L}\left[\left(\frac{R_o}{R}\right)^2 - 1\right] \\ \dot{U}_y &= \dot{U}\left(1 - \frac{Y}{L}\right) \\ \dot{U}_\theta &= 0 \end{aligned} \tag{12}$$

This is an equivalent velocity field to the one presented by Avitzur and Van Tyne (29) in their analysis of ring forming.

For zone II

$$\begin{aligned} \dot{U}_R &= -\frac{\dot{U}R}{2W}\left[\left(\frac{R_o}{R}\right)^2 - 1\right] \\ \dot{U}_y &= \dot{U}\left[1 - \frac{Y}{W}\left[1 + \frac{R}{2W}\frac{\partial W}{\partial R}\left(\left(\frac{R_o}{R}\right)^2 - 1\right)\right]\right] \\ \dot{U}_\theta &= 0 \end{aligned} \tag{13}$$

where

$$\frac{W}{R_i} = \frac{L}{R_o}\frac{R_o}{R_i} + \cot\alpha\left(\frac{R_a}{R_i} - \frac{R}{R_i}\right) \tag{14}$$

This is the equation which describes the relative position

of the die surface (i.e. S_a in Figure 7).

For zone III

$$\dot{U}_R = -\frac{\dot{U}R}{2\bar{Z}}\left[1 - \left(\frac{\delta}{R}\right)^2\right]\left[\frac{\left(\frac{R_o}{R_i}\right) - 1}{1 - \left(\frac{\delta}{R}\right)^2}\right]$$

$$\dot{U}_y = \dot{U}\left[1 + \frac{y}{\bar{Z}}\left(1 - \frac{R}{2\bar{Z}}\frac{\partial Z}{\partial R}\left(1 - \left(\frac{\delta}{R}\right)^2\right)\frac{\left(\frac{R_o}{R_i}\right)^2 - 1}{1 - \left(\frac{\delta}{R_i}\right)^2}\right)\right] \qquad (15)$$

$$\dot{U}_\theta = 0$$

This is equivalent to the velocity field for a similarly shaped zone as presented by Gordon and Van Tyne (8).

For zone IV

$$\dot{U}_R = 0$$

$$\dot{U}_y = v_f = \frac{\dot{U}\left[\left(\frac{R_o}{R}\right)^2 - \left(\frac{\delta}{R_i}\right)^2\right]}{1 - \left(\frac{\delta}{R_i}\right)^2} \qquad (16)$$

$$\dot{U}_\theta = 0$$

By using the upper bound approach, the internal power

of deformation for a perfectly plastic material is determined from the following equation:

$$\dot{W}_i = \int_V \frac{2\sigma_o}{\sqrt{3}} \sqrt{\frac{1}{2}\dot{\varepsilon}_{ij}\dot{\varepsilon}_{ij}}\, dV \tag{17}$$

where V is the volume of the material, and,

the $\dot{\varepsilon}_{ij}$ is a strain rate component.

For zone I, the internal power of deformation is

$$\dot{W}_{i_I} = \frac{\sigma_o \pi \dot{U}}{\sqrt{3}} R_o^2 \left[2 - \sqrt{3\left(\frac{R_a}{R_o}\right)^4 + 1} + \ln\left(\left(\frac{R_o}{R_a}\right)^2 \frac{1 + \sqrt{3\left(\frac{R_a}{R_o}\right)^4 + 1}}{3} \right) \right] \tag{18}$$

This is the equivalent internal power of deformation as the one presented for ring forming by Avitzur and Van Tyne (29).

For zone II

$$\dot{W}_{i_{II}} = \frac{\sigma_o}{\sqrt{3}} \pi \dot{U} R_o^2 \int_1^{R_a/R_i} \frac{p}{2} \left[\sqrt{1 + B} + B \ln \left(1 + \frac{\sqrt{1 + B}}{\sqrt{B}} \right) \right] \rho \, d\rho \tag{19}$$

where

$$B = \frac{(f + 2 + \gamma)^2 + f^2 + (2 + \gamma)^2}{p^2/2} \tag{20}$$

and

$$p = 2\gamma V_{II} + (f + 4) V_{II} - f\rho \frac{\partial V_{II}}{\partial \rho} \tag{21}$$

with

$$\rho = \frac{R}{R_i}$$

$$V_{II} = \frac{\partial W}{\partial R}$$

$$f = \left(\frac{R_o}{R_i} \right)^2 \frac{1}{\rho} - 1 \tag{22}$$

$$\gamma = \rho f V_{II} \frac{R_i}{W}$$

This power term requires a numerical integration to obtain a specific value for it as a function of the process parameters.

For zone III

$$\dot{W}_{i_{III}} = \frac{\sigma_o}{\sqrt{3}}\pi\dot{U}R_o\left(\frac{R_i}{R_o}\right)\left[\frac{\left(\frac{R_o}{R_i}\right) - 1}{1 - \left(\frac{\delta}{R_i}\right)^2}\right] \cdot \int_{\delta/R_i}^{1} \frac{q}{2}\left[\sqrt{1 + A} + A\ln\left(1 + \frac{\sqrt{1 + A}}{A}\right)\right]\rho d\rho \tag{23}$$

where

$$A = \frac{(2 - e - \beta)^2 + e^2 + (2 - \beta)^2}{q^2/2} \tag{24}$$

and

$$q = -2V_{III}\beta + (4 - e)V_{III} + e\rho\frac{\partial V_{III}}{\partial \rho} \tag{25}$$

with

$$\rho = \frac{R}{R_i}$$

$$V_{III} = \frac{\partial Z}{\partial R} \qquad (26)$$

$$e = 1 - \frac{1}{\rho^2}\left(\frac{\delta}{R_i}\right)^2$$

$$\beta = \rho e V_{III} \frac{R_i}{Z}$$

This internal power of deformation is equivalent to the one presented by Gordon and Van Tyne (8) for a similarly shaped zone. A numerical integrations is required to solve for values of this power term.

Zone IV is assumed to move as a rigid body, therefore there is no deformation and no internal power of deformation in this zone.

There are internal shear losses along the surfaces of velocity discontinuity. These power losses can be calculated by the following equation:

$$\dot{W}_s = \int_{S_T} \frac{\sigma_o}{\sqrt{3}} |\Delta v| \, dS \qquad (27)$$

where S_Γ is the surface between the two regions, and,

Δv is the tangential velocity difference that exists along the surfaces.

For the surface Γ_1, between zone I and zone II,

$$\dot{W}_{S_{\Gamma_1}} = \frac{\pi\sigma_o\dot{U}}{\sqrt{3}} \frac{1}{2} R_o^2 \left(\frac{R_a}{R_o}\right)^2 \cot\alpha \left[\left(\frac{R_o}{R_a}\right)^2 - 1\right] \tag{28}$$

For the surface Γ_2, between zone II and zone III

$$\dot{W}_{S_{\Gamma_2}} = \frac{\pi\sigma_o}{\sqrt{3}} R_o^2 \left[\left(\frac{R_o}{R_i}\right)^2 - 1\right] \left[\left(\frac{L}{R_i}\right) + \left(\frac{R_a}{R_i} - 1\right)\cot\alpha \left(\frac{1}{\left(\frac{R_o}{R_i}\right)^2 - 1} + \frac{1}{1 - \left(\frac{\delta}{R_i}\right)^2}\right) + \frac{1}{2}\left(-\cot\alpha - V_{III}\big|_{R_i}\right)\right] \tag{29}$$

where

$$V_{III}\Big|_{R_i} = \frac{L + (R_a - R_i)\cot\alpha}{(R_i - \delta)} \tag{30}$$

For the surface Γ_3, between zone III and zone IV,

$$\dot{W}_{S_{\Gamma_3}} = \int_{\delta}^{R_i} \frac{\sigma_o}{\sqrt{3}} \left| \left[\dot{U} \frac{(\frac{R_o}{R_i})^2 - (\frac{\delta}{R_i})^2}{1 - (\frac{\delta}{R_i})^2} \frac{V_{III}}{\sqrt{1 + V_{III}^2}} \right.\right.$$

$$- \dot{U}\left[1 + \frac{Z}{y}\left(1 - \frac{R}{2Z} V\left(1 - (\frac{\delta}{R})^2\right) \frac{(\frac{R_o}{R_i})^2 - (\frac{\delta}{R_i})^2}{1 - (\frac{\delta}{R_i})^2}\right) \frac{V_{III}}{\sqrt{1 + V_{III}^2}}\right] \tag{31}$$

$$\left.\left. + \dot{U}\left[\frac{R}{2Z}\left(1 - (\frac{\delta}{R})^2\right) \frac{(\frac{R_o}{R_i})^2 - 1}{1 - (\frac{\delta}{R_i})^2} \frac{1}{\sqrt{1 + V_{III}^2}}\right]\right] \right| \sqrt{1 + V_{III}^2}\, RdR$$

where

$$V_{III} = \frac{\partial Z}{\partial R} = \frac{\frac{L}{R} + (\frac{R_a}{R} - 1)\cot\alpha}{1 - \frac{\delta}{R}} \tag{32}$$

The friction power losses along a workpiece/tool interface can be determined from the following equation:

$$\dot{W}_f = \int_S \frac{m\sigma_o}{\sqrt{3}} |\Delta v| \, dS \tag{33}$$

where m is the constant friction factor,

Δv is tangential velocity difference between the tool and the workpiece and S is the interfacial surface.

The friction power losses along S_a, between zone II and the die are

$$\begin{aligned} \dot{W}_{f_a} = \frac{m\sigma_o}{\sqrt{3}} \frac{\pi \dot{U} R_o^2}{\sin\alpha\cos\alpha} \Bigg[\Bigg[1 - \left(\frac{L/R_o}{\cot\alpha} + \frac{R_a}{R_o} \right)^2 \Bigg] \\ \cdot \ln \left(\frac{\frac{L/R_o}{\cot\alpha} + \frac{R_a}{R_o} - \frac{R_i}{R_o}}{\frac{L/R_o}{\cot\alpha}} \right) + \frac{1}{2} \left(\frac{L/R_o}{\cot\alpha} \right)^2 \\ - \frac{1}{2} \left(\frac{L/R_o}{\cot\alpha} + \frac{R_a}{R_o} - \frac{R_i}{R_o} \right)^2 \\ + 2 \left(\frac{L/R_o}{\cot\alpha} + \frac{R_a}{R_o} \right) \left(\frac{R_a}{R_o} - \frac{R_i}{R_o} \right) \Bigg] \end{aligned} \tag{34}$$

The friction power losses along S_b, between zone I and the die are

$$\dot{W}_{f_b} = \frac{m\sigma_o\pi}{\sqrt{3}}\dot{U}R_o^2\left(\frac{R_o}{L}\right)\left[\frac{2}{3} - \frac{R_a}{R_o} + \frac{1}{3}\left(\frac{R_a}{R_o}\right)^3\right] \tag{35}$$

The friction power losses along S_c, between zone I and the chamber are

$$\dot{W}_{f_c} = \frac{m\sigma_o}{\sqrt{3}}\pi\dot{U}R_o^2\left(\frac{L}{R_o}\right) \tag{36}$$

The friction power losses along S_d, between zone I and the ram, are equal to the frictional power losses along surface S_b. Therefore,

$$\dot{W}_{f_d} = \frac{m\sigma_o}{\sqrt{3}}\pi\dot{U}R_o^2\left(\frac{L}{R_o}\right) \tag{37}$$

The friction power losses along S_e, between zone II and the ram are

$$\dot{W}_{f_e} = \frac{m\sigma_o\pi}{\sqrt{3}}\dot{U}R_o^2\tan\alpha\left[\left(1 - \left(\frac{L}{R_o}\tan\alpha + \frac{R_a}{R_o}\right)\right)\right.$$
$$\cdot \ln\left[\frac{\frac{L}{R_o}\tan\alpha + \left(\frac{R_a}{R_o} - \frac{R_i}{R_o}\right)}{\frac{L}{R_o}\tan\alpha}\right] + 3\frac{L}{R_o}\tan\alpha\left(\frac{R_a}{R_o} - \frac{R_i}{R_o}\right) \qquad (38)$$
$$\left. + \frac{1}{2}\left(\frac{R_a}{R_o} - \frac{R_i}{R_o}\right)^2 + 2\frac{R_a}{R_o}\left(\frac{R_a}{R_o} - \frac{R_i}{R_o}\right)\right]$$

The friction power losses along S_f, between zone III and the ram are

$$\dot{W}_{f_f} = m\frac{\sigma_o}{\sqrt{3}}\pi\dot{U}R_o^2\left(\frac{R_i}{R_o}\right)^3\frac{1}{2}\frac{\left[\left(\frac{R_o}{R_i}\right)^2 - 1\right]}{\left[1 - \left(\frac{\delta}{R_i}\right)^2\right]}\frac{\left[\left(1 - \frac{\delta}{R_i}\right)^2\left(1 + 3\frac{\delta}{R_i}\right)\right]}{\left[\frac{L}{R_o} + \left(\frac{R_a}{R_o} - \frac{R_i}{R_o}\right)\cot\alpha\right]} \qquad (39)$$

The upper bound on power is

$$J^* = \dot{W}_{i_I} + \dot{W}_{i_{II}} + \dot{W}_{i_{III}} + \dot{W}_{s_{\Gamma_1}} + \dot{W}_{s_{\Gamma_2}} + \dot{W}_{s_{\Gamma_3}} + \dot{W}_{f_a} + \dot{W}_{f_b} + \dot{W}_{f_c} + \dot{W}_{f_d} + \dot{W}_{f_e} + \dot{W}_{f_f} \tag{40}$$

The total power requirement for the process is supplied by the moving ram. Instead of presenting the influence a change in a process variable has on the value of the J^*, it is more meaningful to relate J^* to the ram pressure and show how the ram pressure is affected. This relationship can be expressed mathematically, as,

$$J^* = \dot{U}\pi p_{AVE} R_o^2 \tag{41}$$

where p_{AVE} is the average ram pressure.

By equating Eq. (41) to the sum of the internal powers of deformation, internal shear power loses and the frictional power loses, the relative average ram pressure can be determined. This would be

$$\frac{P_{AVE}}{\sigma_o} = \frac{J^*}{\dot{U}\pi R_o^2} \tag{42}$$

or in function form

$$\frac{P_{AVE}}{\sigma_o} = \left(\frac{R_o}{R_i}, \frac{L}{R_o}, \frac{R_a}{R_o}, \alpha, m, \& \frac{\delta}{R_i}\right) \tag{43}$$

The above function form shows that the relative average ram pressure is dependent on the geometry of the billet and tooling, the frictional conditions and the pseudo-independent parameter, δ.

4.2 FINITE ELEMENT ANALYSIS

This study uses the finite element code NIKE2D which was developed by Hallquist. NIKE2D is a vectorized implicit, finite deformation, large strain, finite element code for analyzing the response of two-dimensional axisymmetric, plane strain, and plane stress solids (14). A variety of loading conditions can be handled including traction boundary conditions, displacement boundary conditions, concentrated nodal points loads, body force loads due to base accelerations, and body force loads due to spinning. NIKE2D has been applied to a wide range of large deformation, inelastic response calculations, by a number of users and generally, the results have been quite satisfactory.

MAZE (15) is an interactive program that has been developed as a input generator for NIKE2D. This program is used in the present work as the preprocessor for NIKE2D.

ORION (16) is the interactive color post-processor for NIKE2D. ORION reads the binary plot files generated by NIKE2D and plots contours, time histories, and deformed shapes. ORION also can compute strain measures, interfaces pressures along constrained boundaries, and momentum. This post-processor is also utilized in the present work.

The initial geometry which is used in the finite element analysis for the billet and the tooling is shown in Figure 9. The views are cross sections through the three dimensional axisymmetric process. The orientation of the process has been rotated 90° as compared to the schematic shown in Figures 3 and 6. The ram is at the top the diagram and the die is at the bottom . The extrusion is in the downward direction. Different conical die angles are used in the FEM simulations. A die angle of 50° is shown in Figure 9a and an angle of 60° is shown in Figure 9b. For this process, a 50 x 15 rectangular element mesh is used to model the workpiece.

In the finite element model, the material properties need to be defined. An elastic-plastic behavior for the workpiece and an elastic behavior for the ram and chamber are assumed. The specific material properties which are used in the finite element method are given Table 1. These properties are representative of steel for tooling and hot-worked aluminum for the workpiece.

The finite element code NIKE2D uses the Coulombic friction coefficient (μ) to model the interaction between the workpiece and the tool at frictional surfaces. The upper bound analysis uses the constant friction factor (m) for modeling frictional conditions.

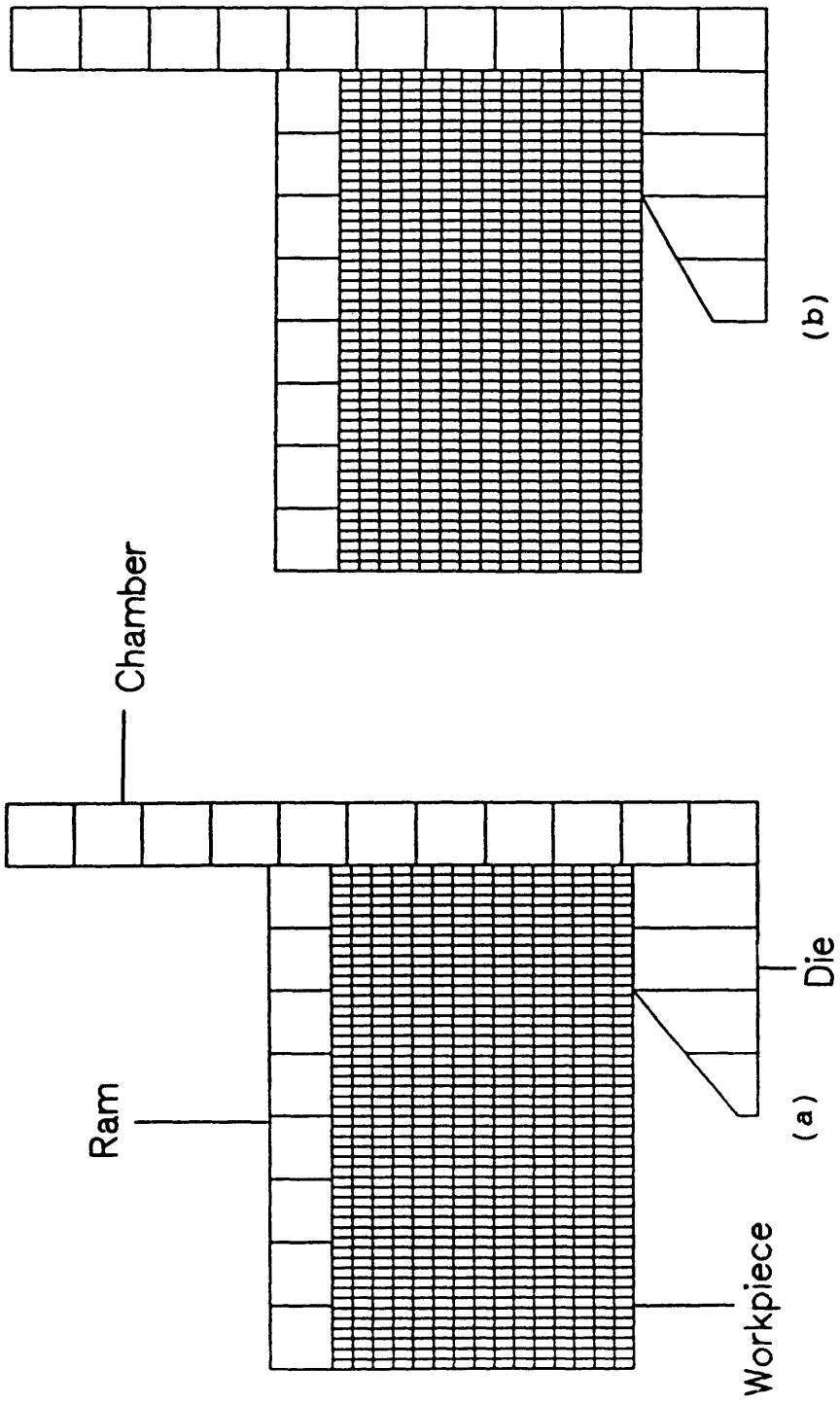

Figure 9 Initial geometry for the finite element analysis of the extrusion process with conical die angles of
(a) α=50° (b) α=60°

	Billet	Die,Ram,Chamber
Flow Type	elastic-plastic	elastic
Elastic Modulus (E)	1.0×10^4 ksi	3.0×10^4 ksi
Yield Strength (σ_{ys})	10 ksi	-
Poisson Ratio (ν)	0.30	0.29
Density (ρ)	0.10 lb/in^3	0.29 lb/in^3
Tangent Modulus (E_T)	1.0×10^3 ksi	-

Table 1 The specific material properties used in the finite element analysis.

5. RESULTS AND DISCUSSION

5.1 UPPER BOUND ANALYSIS

In this section, the results that have been obtained for the upper bound analysis are described. Results from the assumed velocity fields will be presented. First, the characteristics of the sound flow pattern will be described and then the characteristics of the defect flow pattern will be presented. The size of the piping defect as a function of the process parameters is determined. The criteria curves which can be used for the prevention of the piping defect will be generated.

5.1.1 Characteristics of the Process

As a discussed in Section 4, the pseudo-independent parameter used for sound flow is the ε parameter. The δ parameter which is the pipe size is used for defect flow. Using δ as the pipe size only becomes relevant when a defect is present. From a flow-pattern perspective, either parameter can be used as the pseudo-independent variable and would yield the same results. The value of this parameter is determined through the principle of minimum energy. The optimum value of ε is the one at which the ram pressure is a minimum for a given set of process conditions.

Figure 10 shows the individual power terms as a function of the relative pseudo-independent parameter ε/R_i. An enlargement of the scale for the relative average ram pressure is presented in Figure 11. The process geometry for these figures is $L/R_o = 0.45$, $\alpha = 75°$, $R_a/R_o = 0.75$ and $R_i/R_o = 0.50$ with friction m = 0.00. When m is zero (i.e. there is no friction) only internal shear power losses and the internal powers of deformation contribute to the total power. In order to generate these curves Eqns. (19), (22), (23), (28), (29) and (31) are used. These equations incorporate the internal deformation powers and the internal shear power losses. The values generated by these equations are divided by $\dot{U}\ \pi\ R_o^2\ \sigma_o$ in order to present relative power

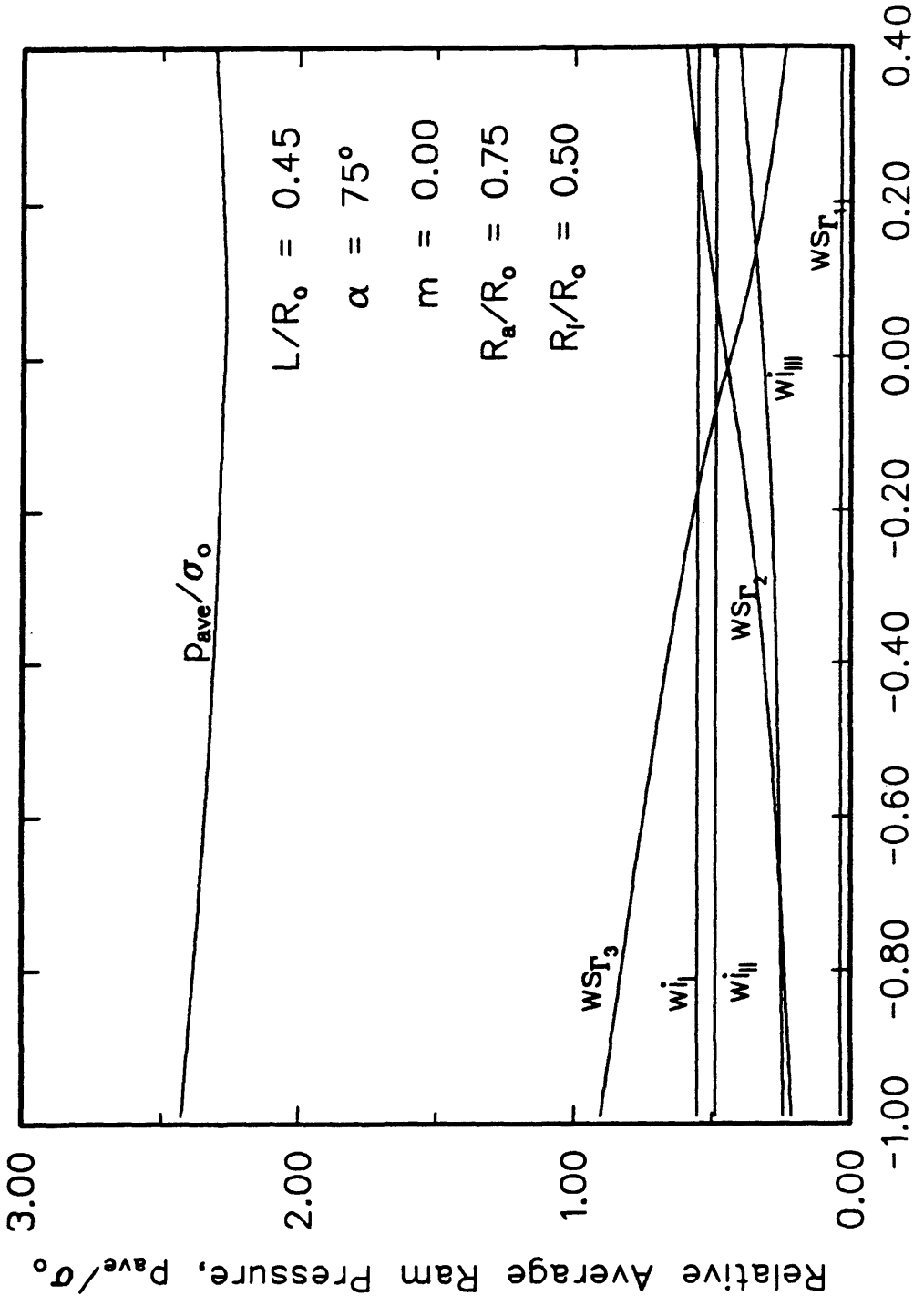

Figure 10 Relative average ram pressure and relative power terms as a function of ε/R_i.

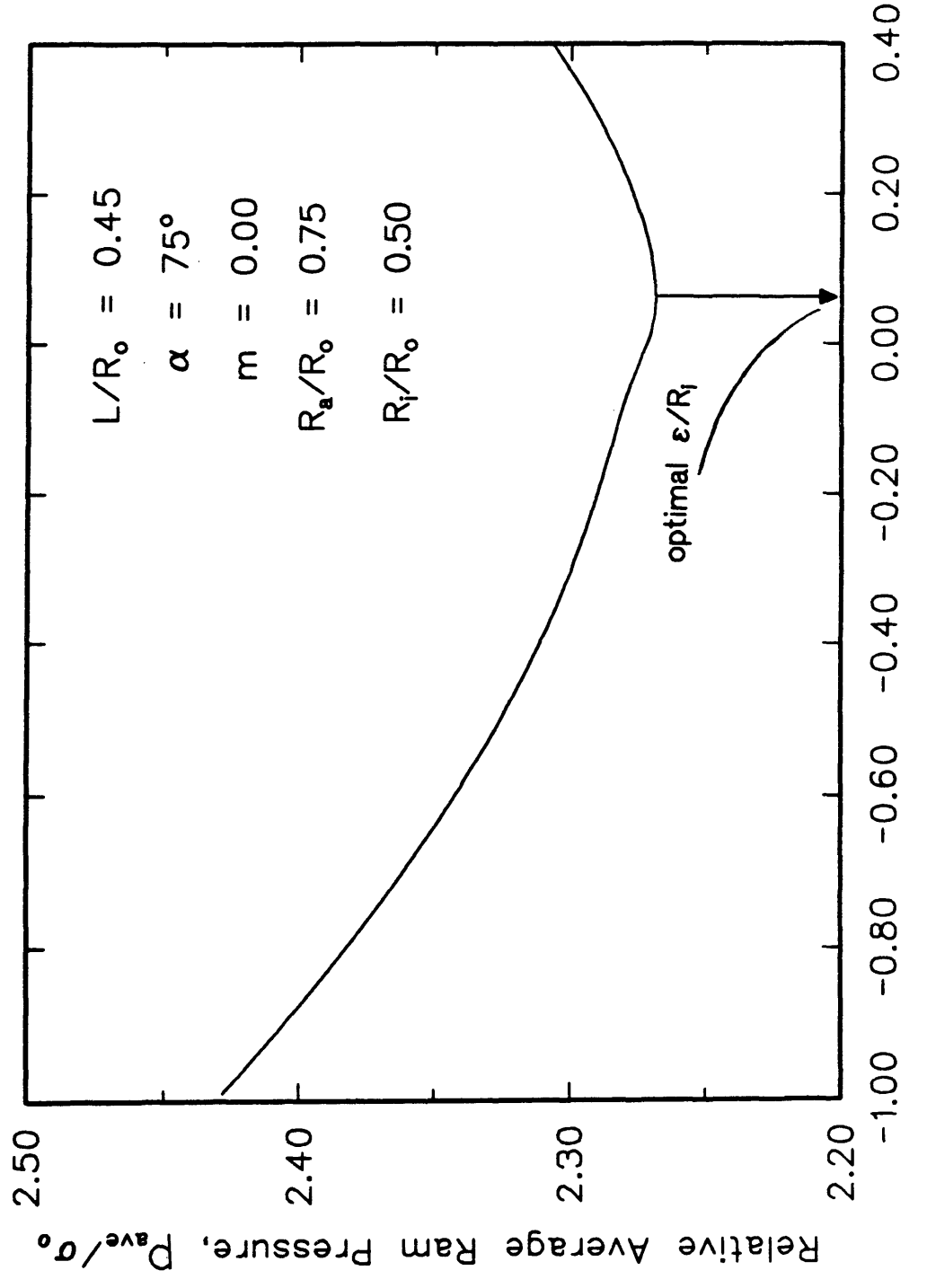

Figure 11 Relative average ram pressure on an expanded scale.

terms which sum to p_{AVE}/σ_o. The internal power of deformation is strongly dependent upon the volume of material being deformed and the internal shear losses are dependent on the area of the internal surfaces of velocity discontinuity. Each of the relative power terms contributes to the total power and their sum provides the overall form of the relative average ram pressure which is needed for the extrusion to occur. Since the upper bound approach has been used the smallest upper bound on power (or the smallest relative pressure) is the one that is most likely to occur.

By plotting the relative average pressure as a function of the pseudo-independent parameter ε, the value of this parameter which requires the minimum power can be readily determined. In order to determine whether sound flow or defect flow will prevail under these process conditions, this minimum value is used. Figure 11 shows the minimum value for the relative average pressure occurs for a value of $\varepsilon/R_i = 0.06$ (i.e. $\varepsilon/R_i > 0$). This positive value of ε/R_i indicates that flow with a piping would not occur for the given values of the independent process parameters.

In Figure 12, the relative power terms are presented in a graphical fashion as a function of the pseudo-independent parameter ε. An expanded scale presentation of the relative average pressure is shown in Figure 13. The geometry for

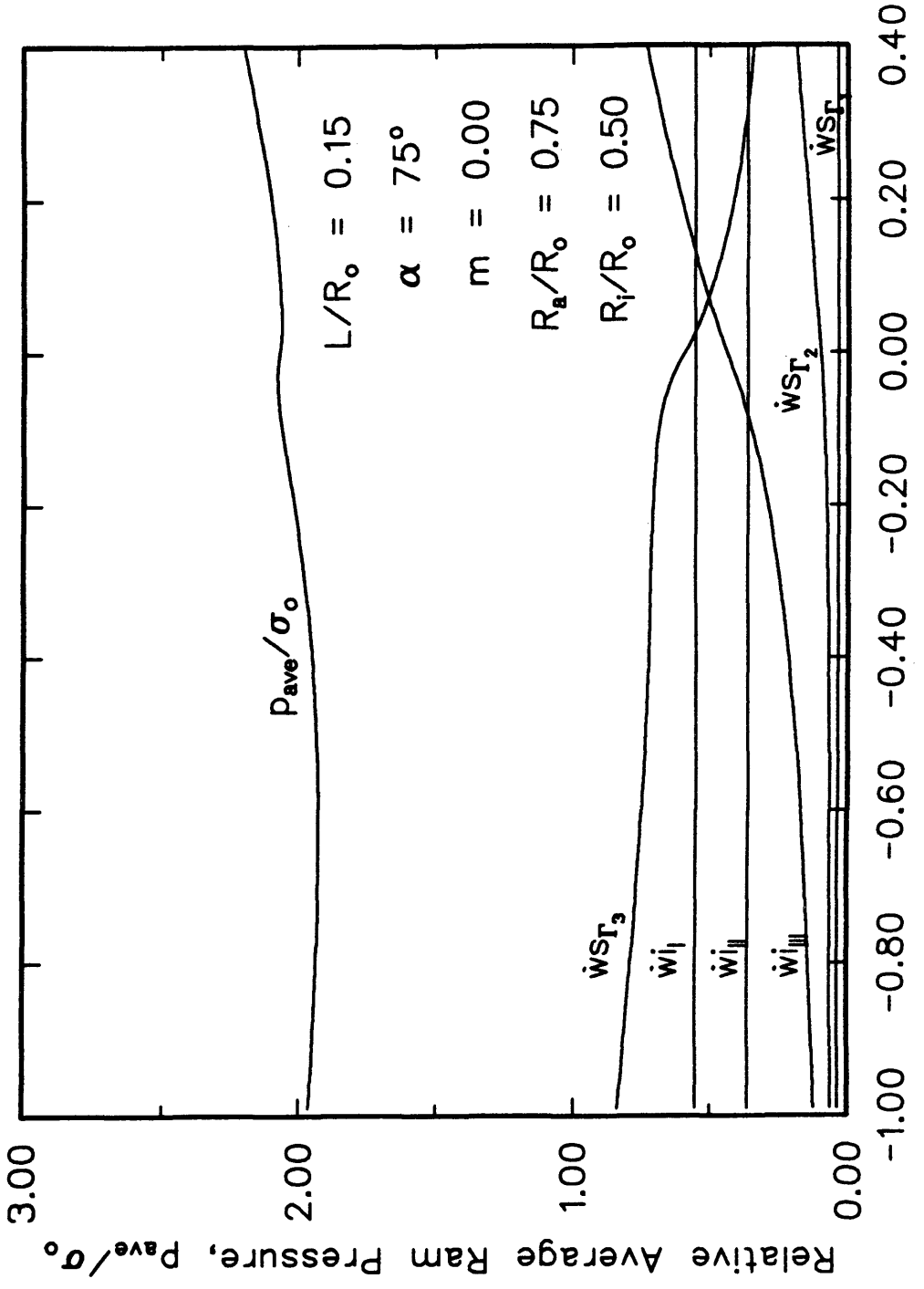

Figure 12 Relative average ram pressure and relative power terms as a function of ε/R_i.

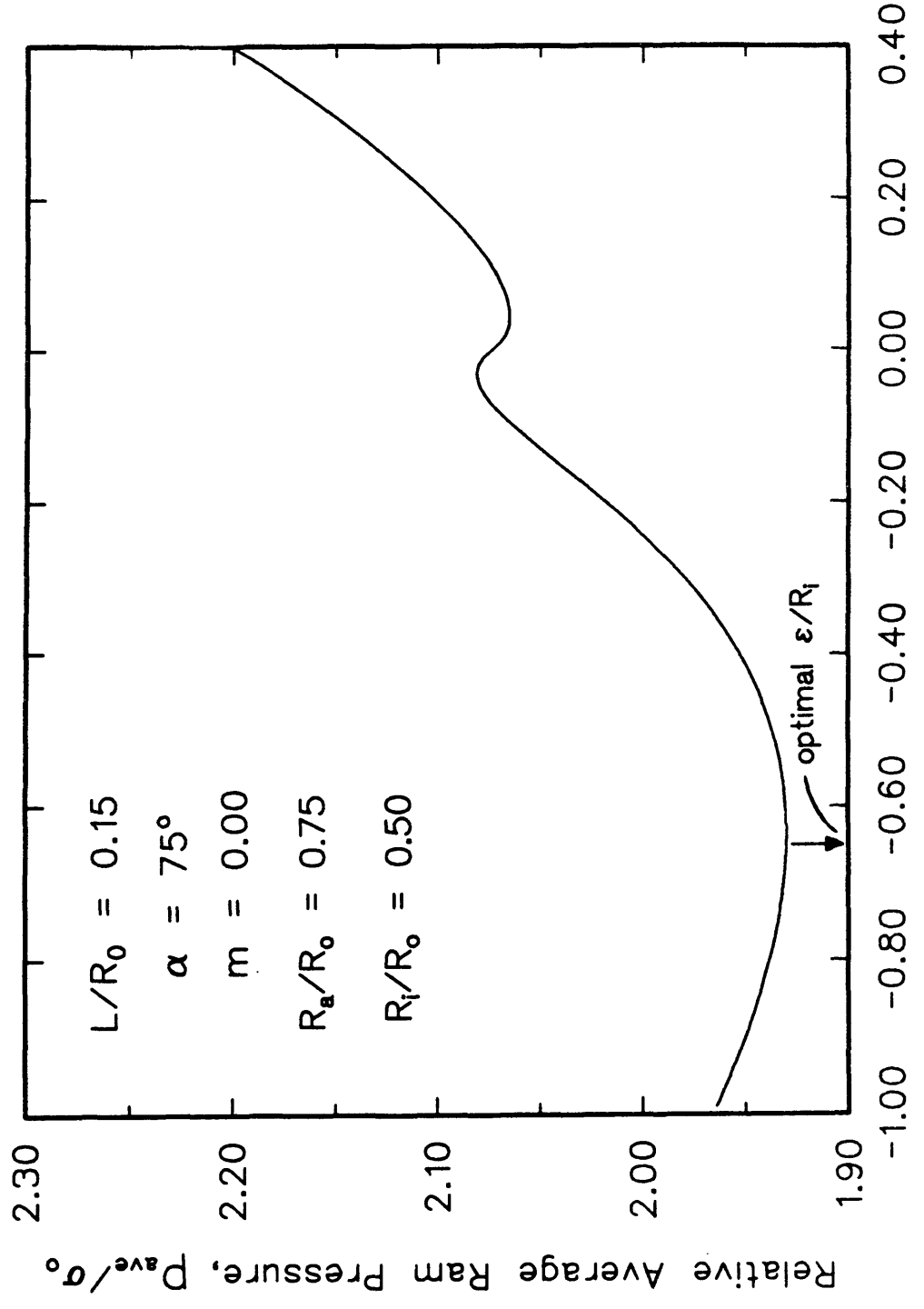

Figure 13 Relative average ram pressure on an expanded scale.

this graph is L/R_o = 0.15, α = 75°, R_a/R_o = 0.75 and R_i/R_o = 0.50 with friction, m = 0.00. These values are the same as for Figures 10 and 11 except for the relative thickness value of 0.15 instead of 0.45. The larger relative thickness should promote sound flow. Figure 13 shows that the minimum value for the relative pressure occurs at ε/R_i = -0.64 (i.e. $\varepsilon/R_i < 0$). Since the optimal ε/R_i is smaller than zero, defect flow would be expected. Also, this figure shows that the negative ε/R_i has a slightly lower relative ram pressure.

The difference between the values used for the independent variables in Figure 10 and Figure 12 is the relative length of the non extruded portion of the billet L/R_o. Figure 10 has L/R_o = 0.45 and Figure 12 has L/R_o = 0.15. This indicates that piping will occur at the end of the stroke when the remaining non extruded billet length becomes small.

From Figure 10, it can be seen that the relative average ram pressure is close to 2.27. When the friction is increased from 0.00 to 1.00, the value of the relative average ram pressure increases 10.56. This indicates that an increase in the friction factor causes a large increase in the relative average ram pressure.

Figure 14 shows the first appearance of a relative

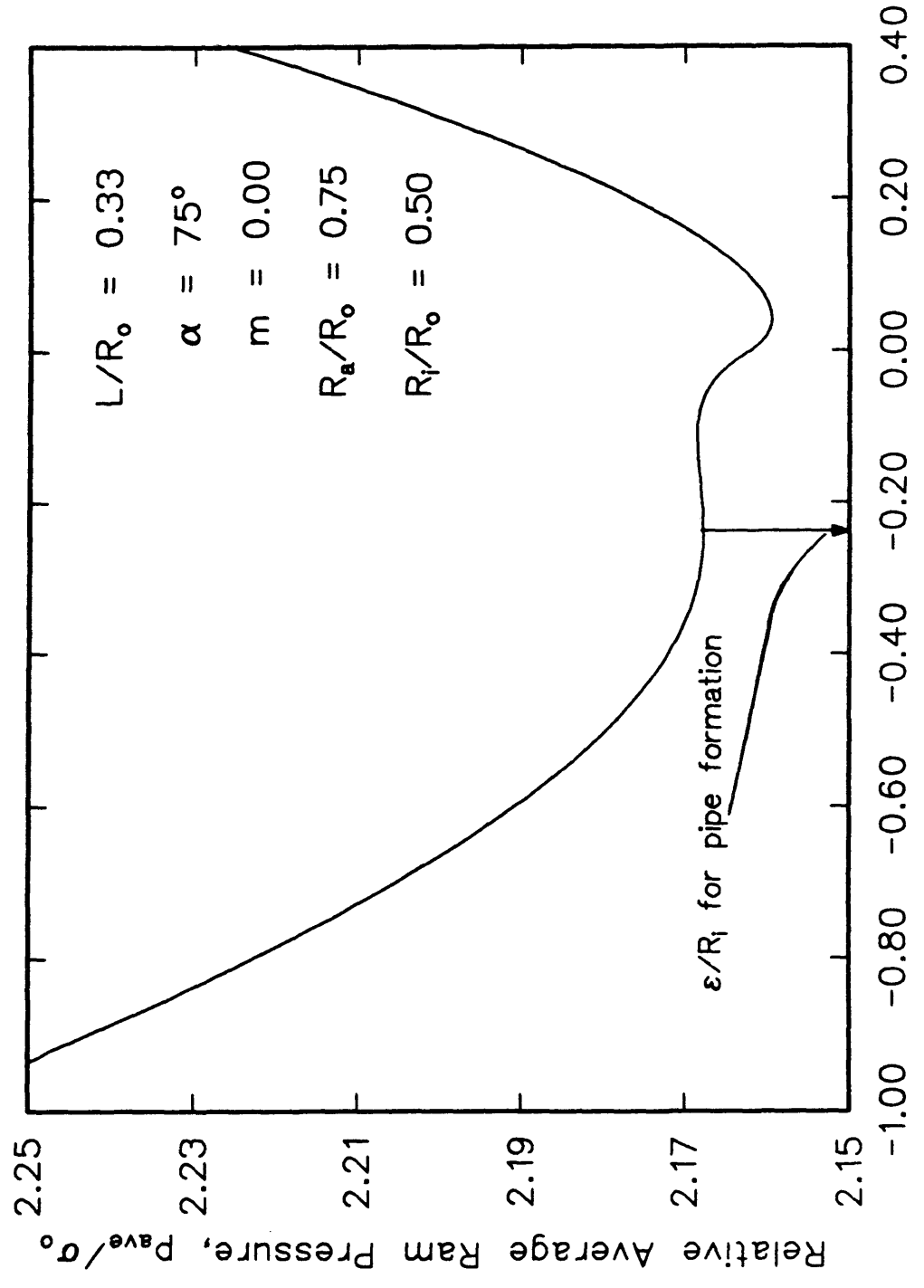

Figure 14 Relative average ram pressure at the transition point between sound flow and defect flow.

minima in the negative ε/R_i region as the value of L/R_o is decreased. Although this is not the true transition point based upon lowest energy consideration. There is still a possibility of a pipe forming at this relative billet length due to the local minima. The presence of a local minima on the negative side of the ε/R_i region will be used in this work as an indication that piping defect is possible.

Figure 15 illustrates the relative pipe size as a function of the relative length of the non extruded portion of the billet. For a given product to billet ratio (R_i/R_o = 0.50), relative radius of the conical region of the die (R_a/R_o = 0.75) and die angle (α = 75°), it is observed that the pipe size increases as the non extruded billet length decreases. This indicates once the pipe commences it will grow larger as the extrusion process continues. This observation is shown experimentally in Figure 11. For different m values, the shape of the curves is similar. When the die angle α is changed from 75° to 60°, Figure 16 is obtained. For the same non extruded billet length, the relative pipe size is smaller with a decrease in die angle α, as seen comparing Figures 15 and 16. If the die angle α becomes 45° as shown in Figure 17, the relative pipe size becomes even smaller for a constant relative length. Therefore, Figure 15, 16 and 17 indicate that for fixed

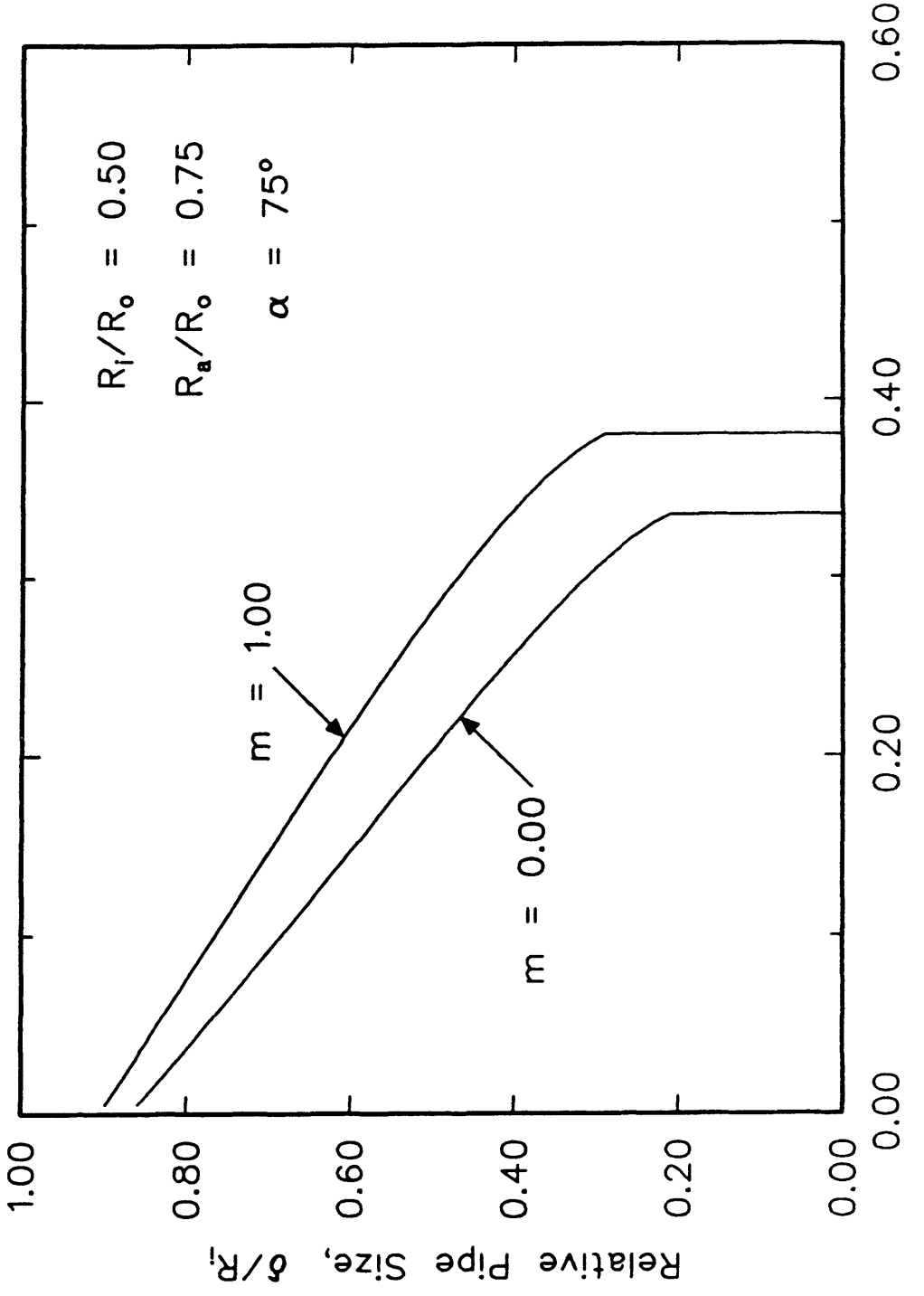

Figure 15 The relative pipe size as a function of relative length of the non extruded portion of the billet for a die angle α=75°.

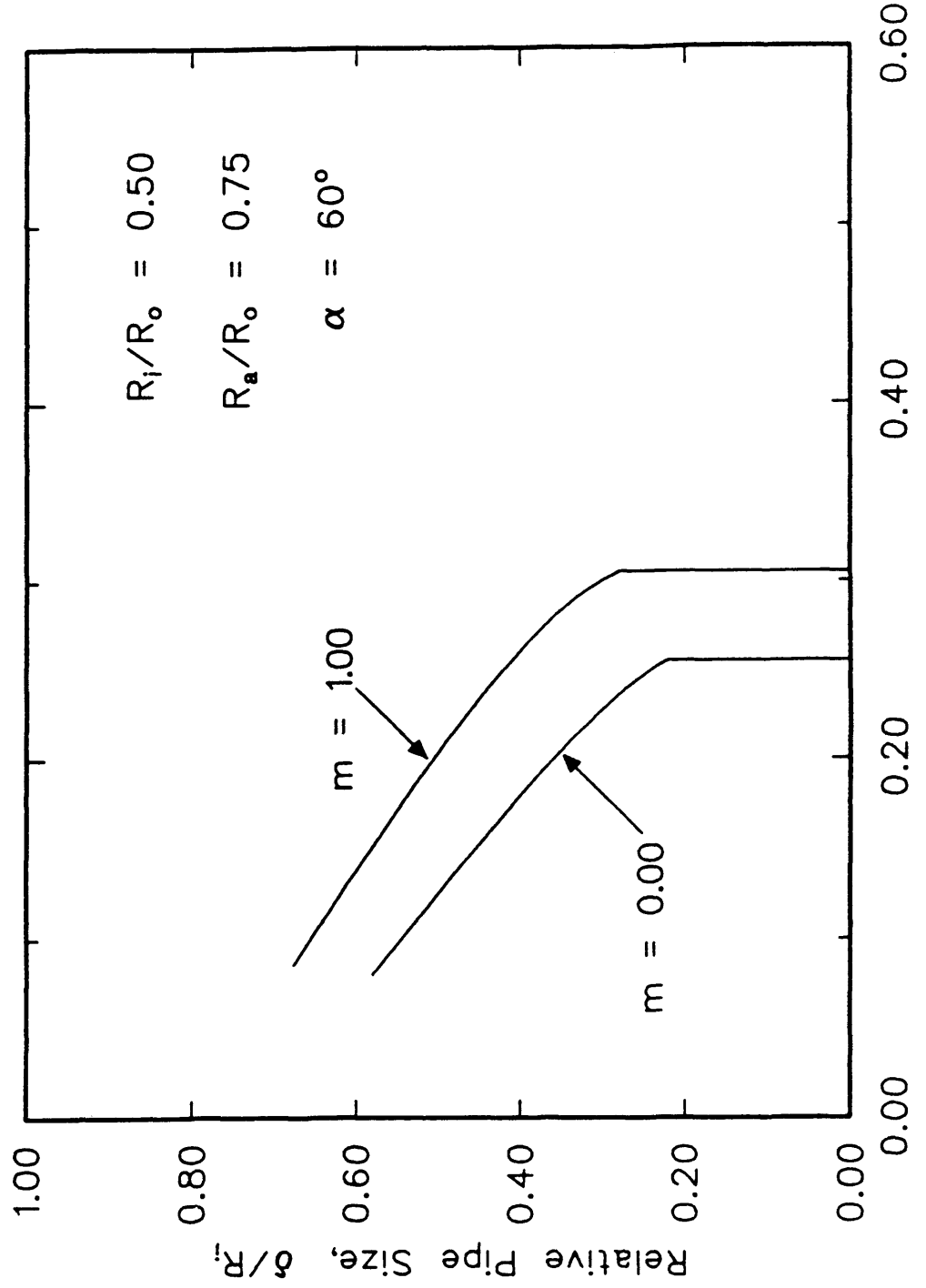

Figure 16 The relative pipe size as a function of relative length of the non extruded portion of the billet for a die angle α=60°.

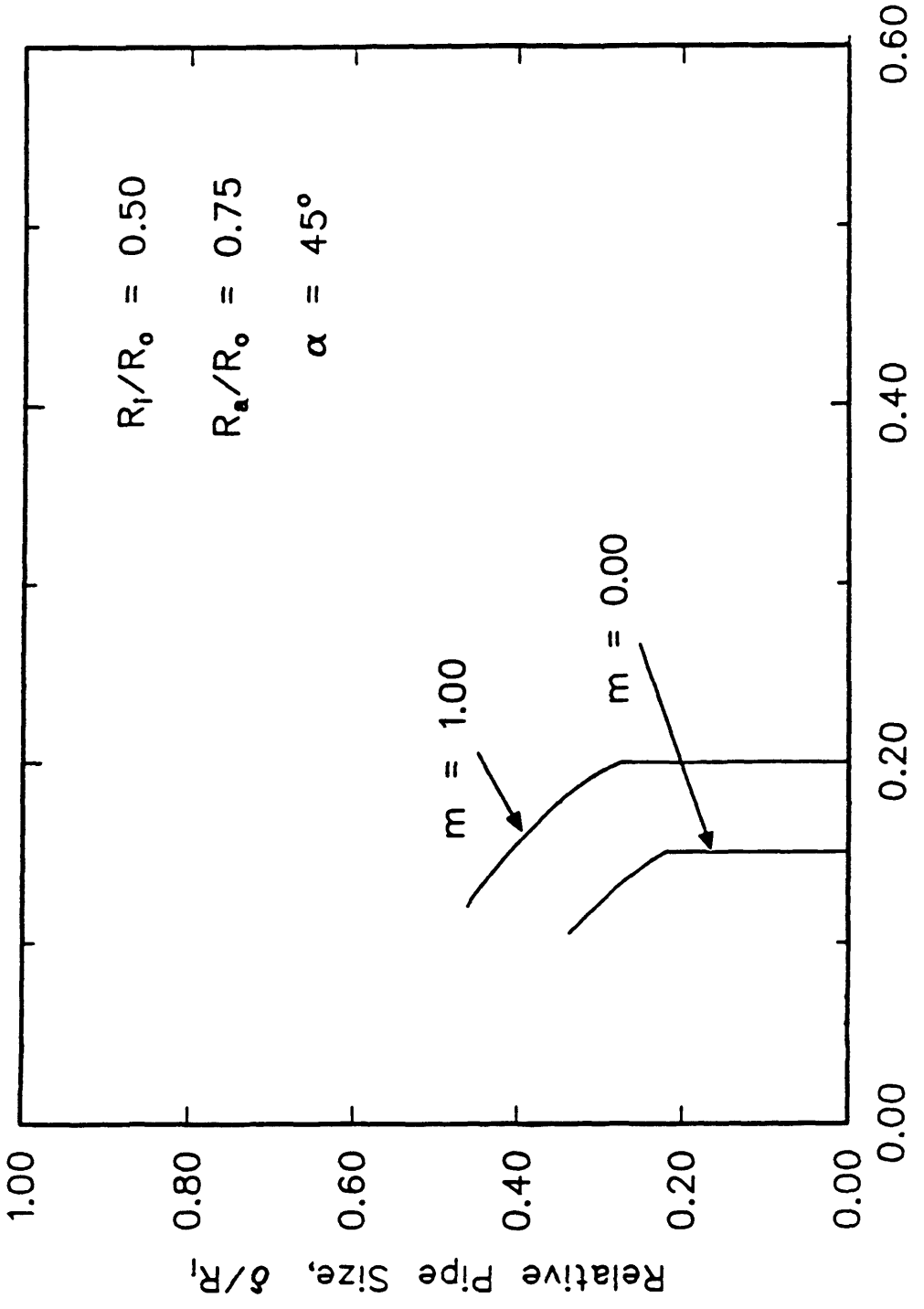

Figure 17 The relative pipe size as a function of relative length of the non extruded portion of the billet for a die angle α=45°.

values of R_i/R_o and R_a/R_o, the relative pipe size decreases with decreasing die angle α.

Although the size of pipe decreases with decreasing die angle, α, there is a limitation to Figures 16 and 17. When the die angle, α, becomes smaller, the validity of the equations used to generate the curves becomes questionable. This behavior is observed in Figure 17. For $L/R_o = 0.10$ and lower, the relative defect size is not shown. The reason for this absence is that the shear power losses along the surface Γ_2 is zero within this region due to a negative axial velocity in zone II. As such, Eq. (29) no longer represents the internal shear power losses along this surface. This behavior needs to be explored further in future work.

5.1.2 Criteria Curves for Defect Prevention

Based upon the upper bound analysis for a perfectly plastic material which is described in Section 5.1.1, the criteria for the formation of the piping defect can be developed. Figure 18 is one set of curves. These curves are a summary plot of all the transition points from sound flow to defective flow as a function of processing parameters. In Figures 18, 19 and 20, the conical die angle, α, is plotted on the abscissa and the relative length of the non extruded portion of the billet is plotted on the ordinate. Curves for various friction factors are shown. When the processing conditions are above or to the left of the curve, sound flow (no pipe) is favorable. When the processing conditions are to the right or below the curve, defect flow is energetically favorable and under these conditions the formation of a pipe is possible.

For a fixed die (i.e. constant α and R_a) and a fixed reduction (i.e. constant R_i and R_o), the only geometrical parameter that would be changing as the extrusion process occurs is the length of the non extruded portion of the billet. This length (L) would be decreasing as the process occurs. The extrusion would occur with no pipe and would produced downward along a constant α line in Figure 18. At same point the remaining billet length would be short enough

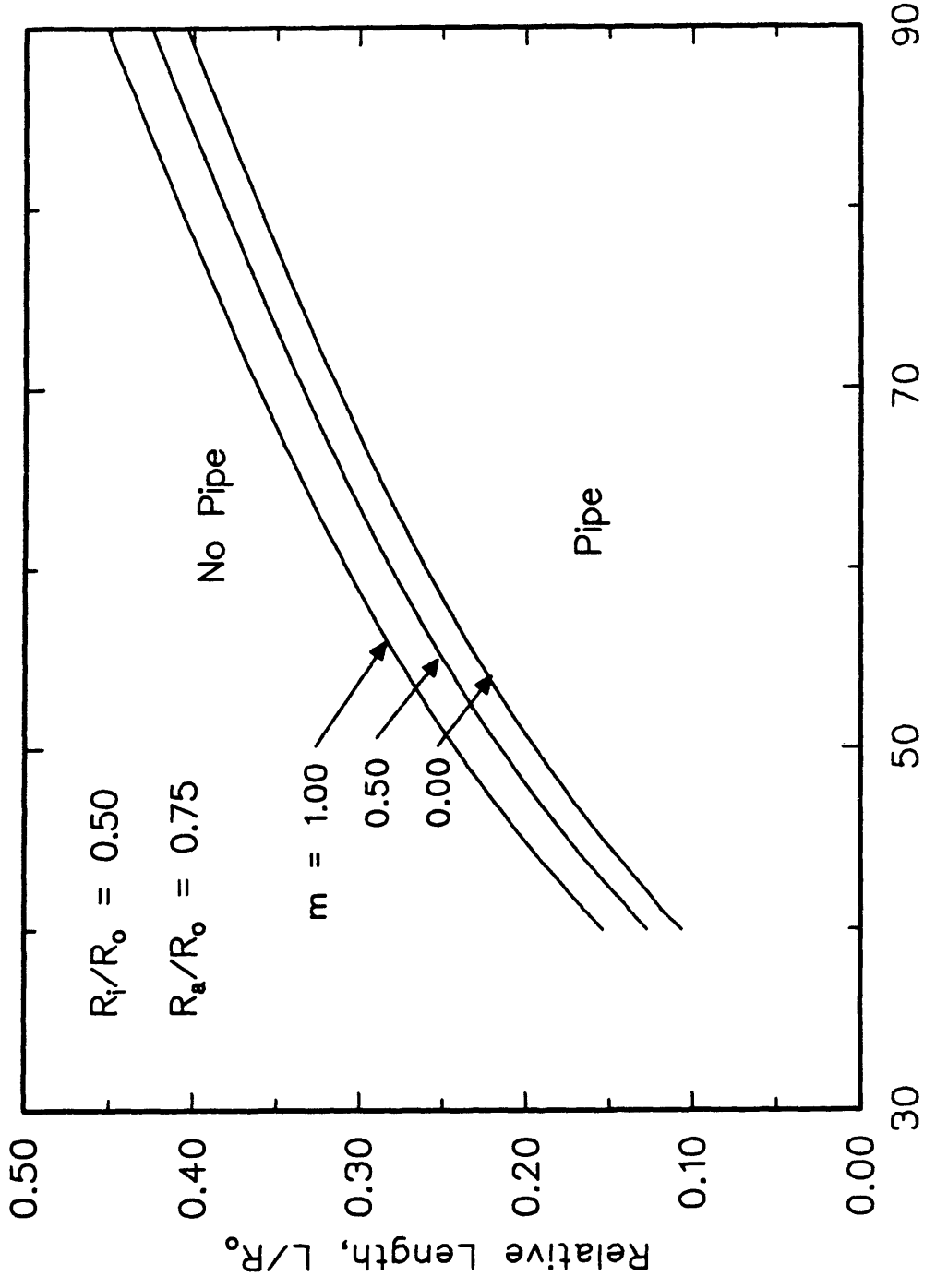

Figure 18 Criteria curve for piping defect formation.

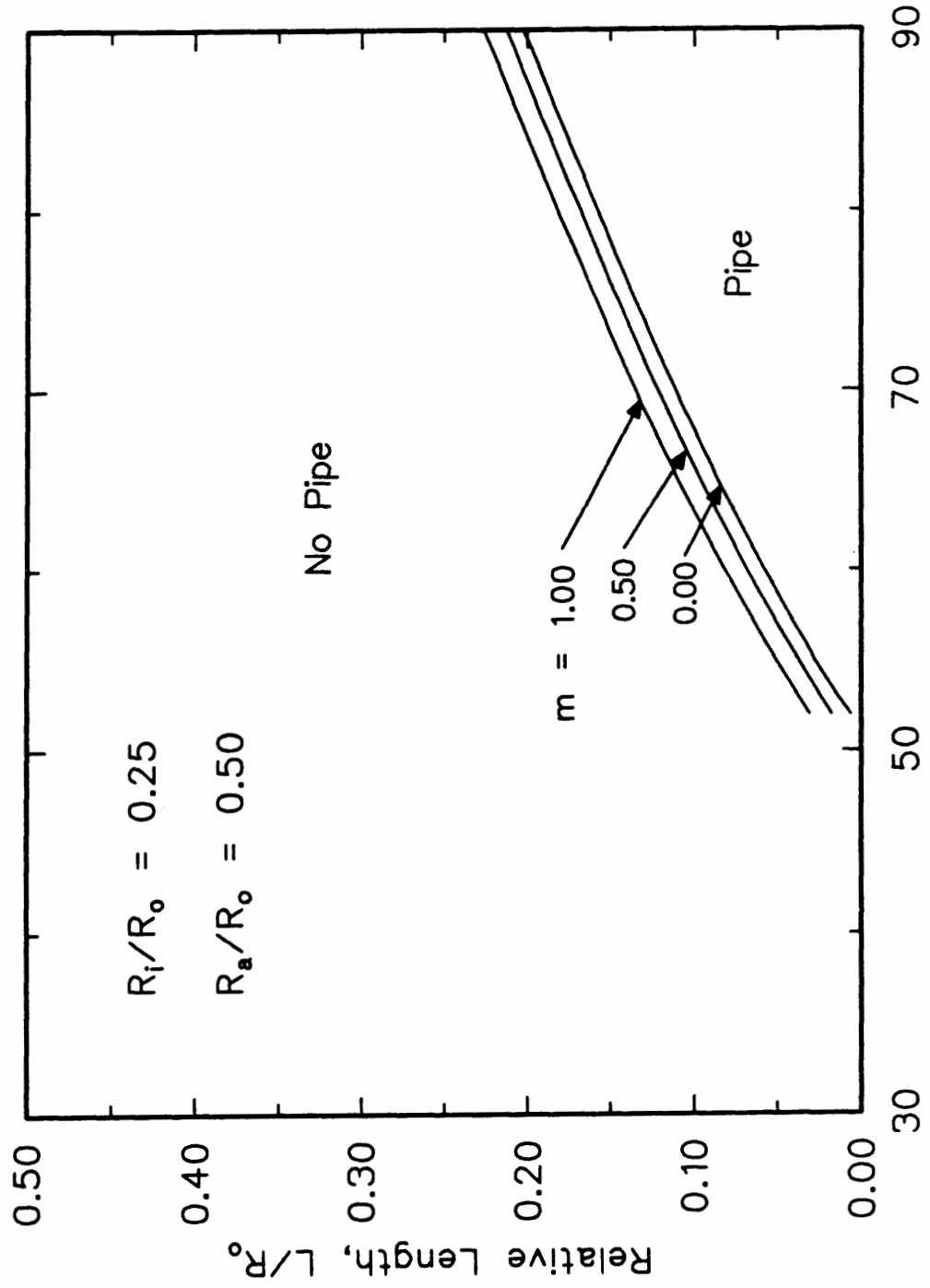

Figure 19 Criteria curve for piping defect formation.

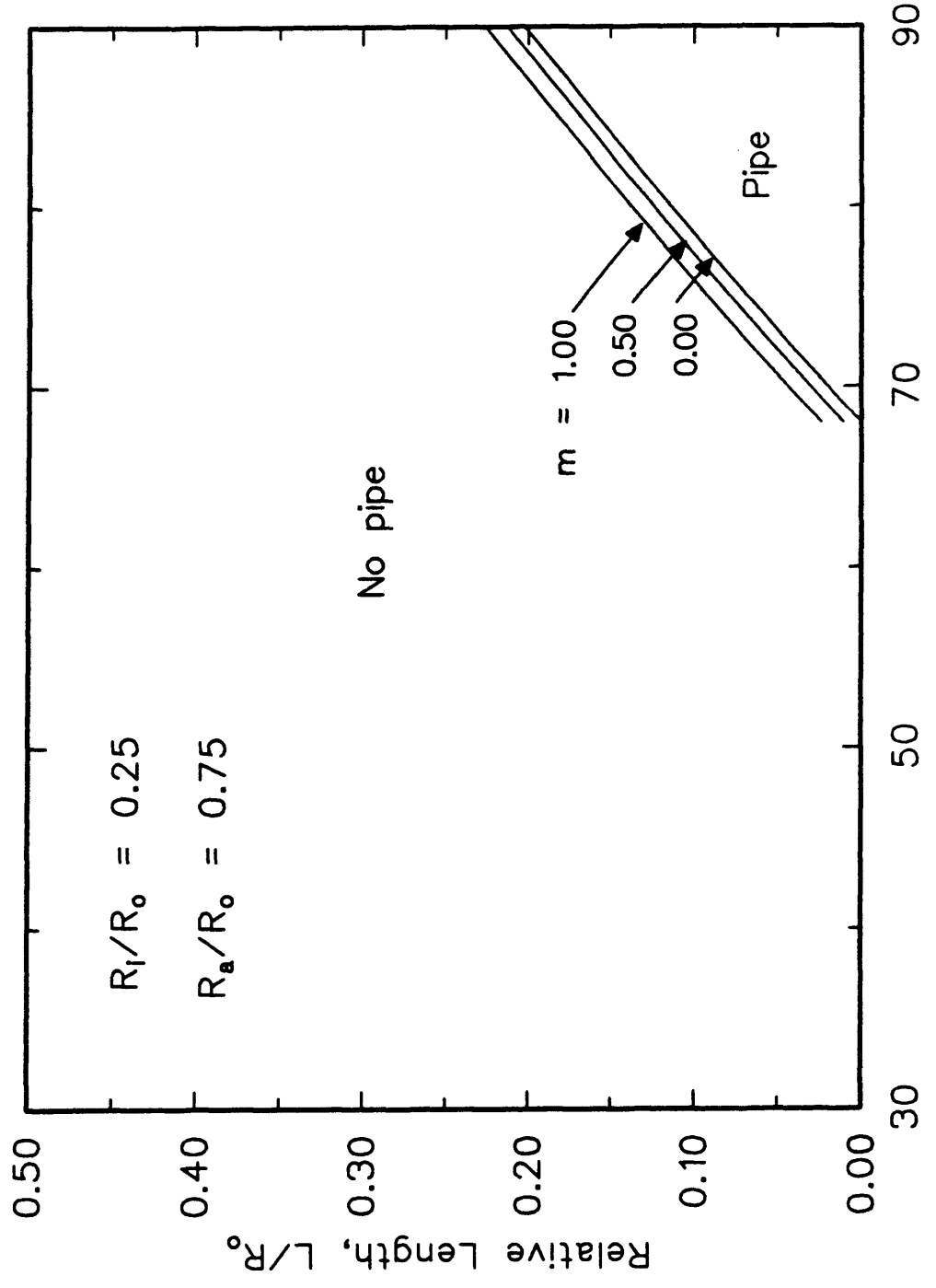

Figure 20 Criteria curve for piping defect formation.

that the curve separating pipe from no pipe behavior is cross. At this time a pipe would begin to develop in the billet.

From a manufacturing perspective, one would like to maximize the length of product produced which does not have a pipe. This is equivalent to determine the process conditions that would cause no pipe region to increase in size. The effect of the processing parameters of die, reduction ratio and friction are examined in the next several figures.

In Figure 18, it can be easily seen that increasing friction increases the domain for piping. In other words, at lower friction conditions with constant die angle the work-piece is less likely to form a pipe. Friction plays a small role in causing the piping defect. When the relative length of the non extruded portion of the billet (i.e. the value of L/R_o) is fixed by going to a smaller die angle (i.e. decreasing the value of α), the expected region for piping becomes smaller.

If the inverse reduction ratio (i.e. the value of R_i/R_o) and the relative radius of the conical region of the die (i.e. R_a/R_o) are changed to lower values as shown in Figure 19, the criteria curves move so that the domain for piping is reduced.

When the inverse reduction ratio (i.e. R_i/R_o) is lowered with a high value R_a/R_o, the piping domain becomes even smaller. This condition can be seen in Figure 20. Therefore, if the inverse reduction ratio decreases and the ratio of R_a/R_o increases, the process could move from the danger region, in which piping is expected, to a safe region and the potential for the piping is avoided.

The transition from sound flow to defect flow as a function of relative length of the non extruded portion of the billet and relative radius of the conical region of the die (R_a/R_o) is shown in Figure 21. It is seen that at low R_a/R_o ratios, the piping defect begins at much larger billet lengths.

Figure 22 shows the transition points between sound flow and defect flow as a function of the relative length of the non extruded portion of the billet and the inverse reduction ratio (R_i/R_o). These curves are for a constant value of R_a/R_o but show the variations which occur as the extrusion reduction is changed. The parameter of friction goes from m = 0.00 to its maximum value m = 1.00 on the three curves presented. It is seen that as the inverse reduction ratio increases (i.e. decreased reduction), the relative billet length at which piping first occurs increases.

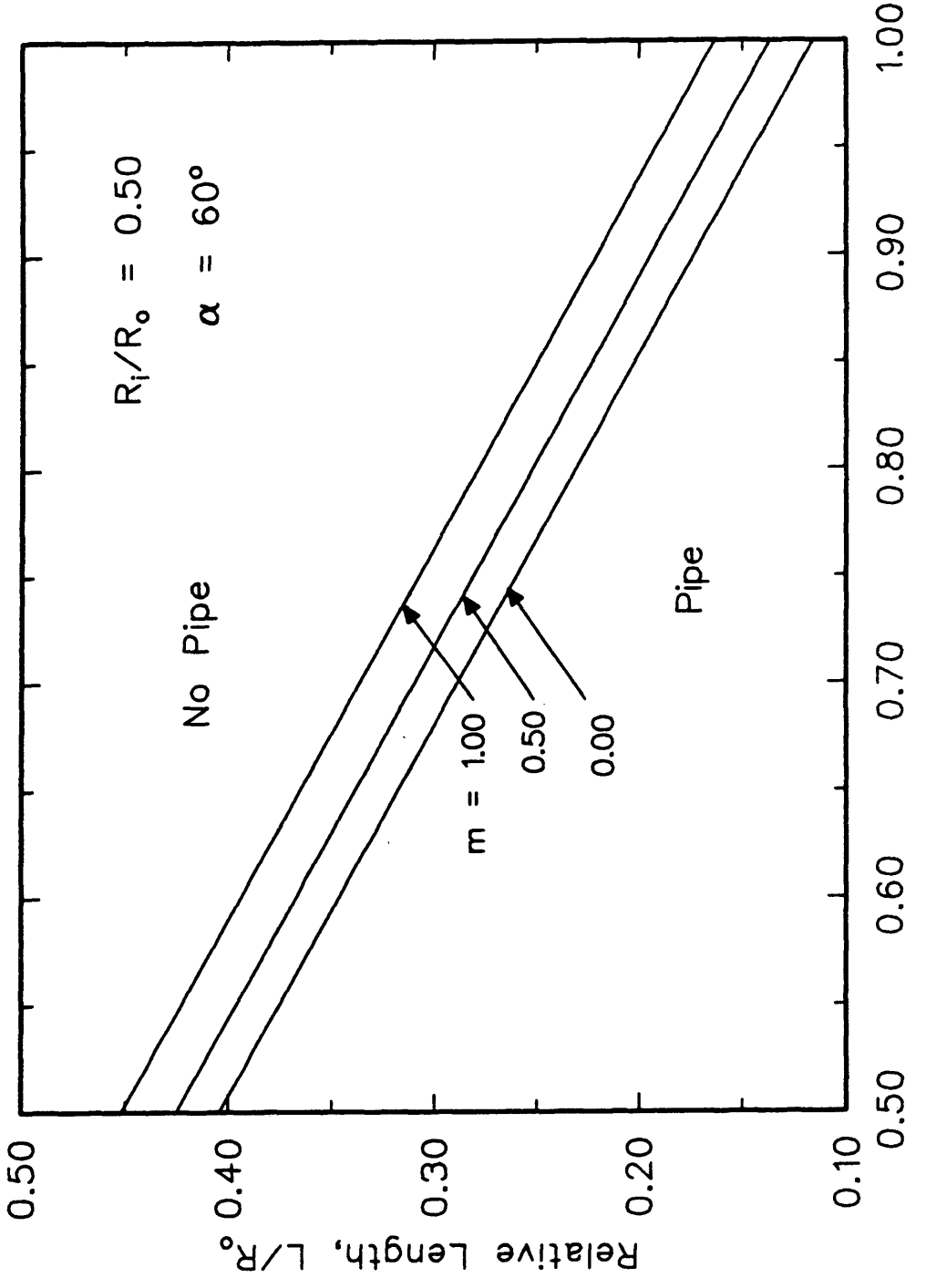

Figure 21 Criteria curve as a function of the relative length of the non extruded portion of the billet and the relative radius of the conical region of the die.

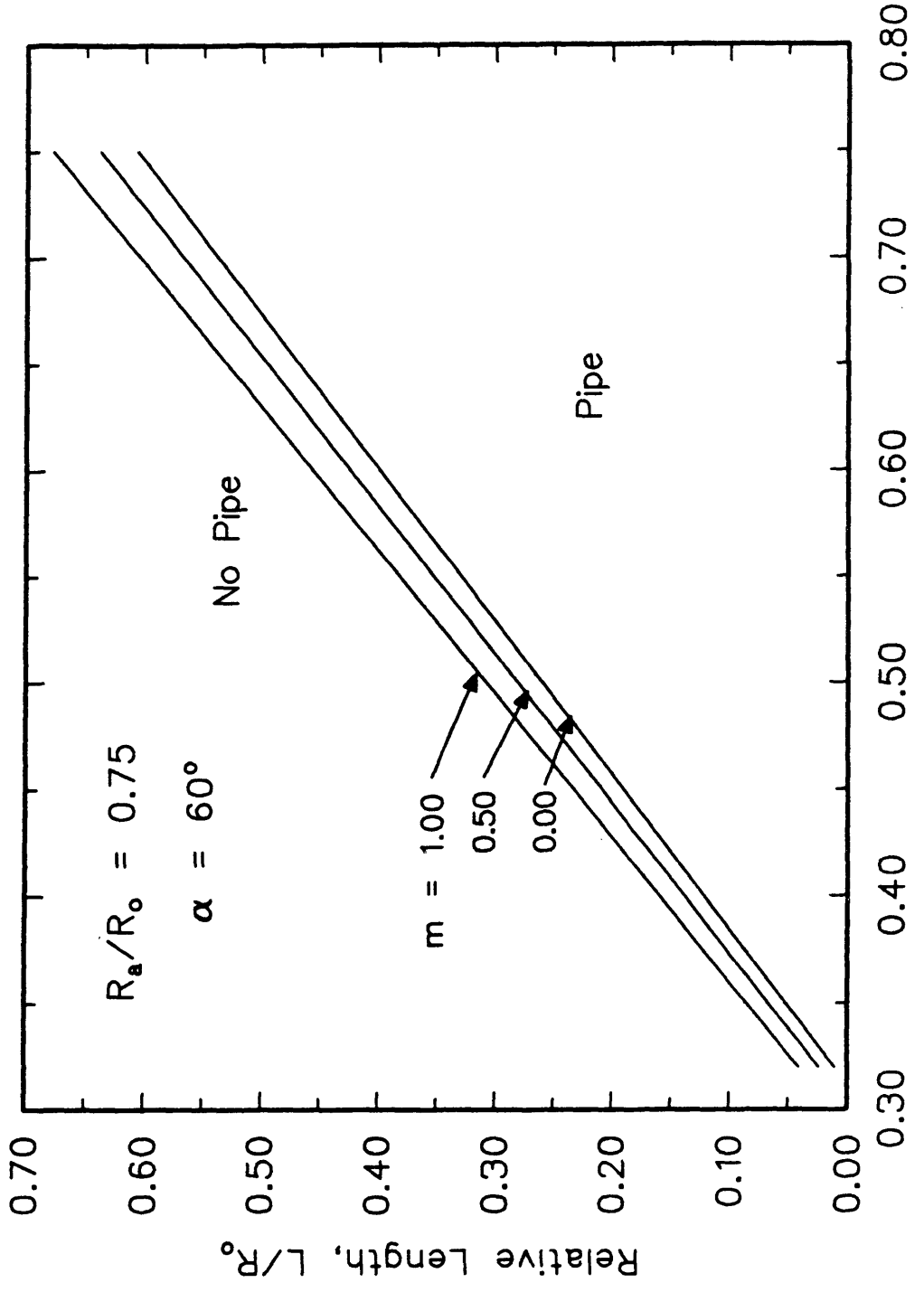

Figure 22 Criteria curve as a function of the relative length of the non extruded portion of the billet and the inverse reduction ratio.

Figures 20 through 22 can be used to determine changes in the process conditions should be made, so that extrusion can be done without the danger of a piping defect. In summary these curves indicate that piping defect can be avoided when non extruded billet length is large, the die angle is small, the inverse reduction ratio, R_i/R_o, is small (i.e. large reduction ratios) and the radius of the conical region of the die, R_a is large.

These criteria can be compared with Johnson's (13), Avitzur's (4) and Gordon & Van Tyne's (8) criterion for piping defect. Based upon Johnson's criterion, a non piping flow forms when the one half the length of the non extruded part of the billet is larger than the product radius (i.e. $R_i > L$). This simple criterion corresponds a straight line in this study. Avitzur showed that the pipe will start at larger non extruded billet length when reduction ratio becomes small. He uses a two zone velocity field with a die angle $\alpha = 90°$. The values obtained from his criteria match the values obtained from this work for die angle $\alpha = 90°$. Gordon and Van Tyne found that at small reduction ratios (i.e. R_i/R_o is large), the pipe will start at larger non extruded billet lengths. They have used a three zone velocity field to examine piping defect at the end of the stroke in extrusions with flat dies (i.e. $\alpha = 90°$). This

work confirms the criteria obtained by Gordon and Van Tyne for flat dies. In addition to flat die, this study also indicates the criteria for the conical die angle changes.

5.2 FINITE ELEMENT METHOD ANALYSIS

This section provides the results and discussion of the finite element analysis. These results are used to confirm the criteria curve obtained from the upper bound analysis which have been presented in Section 5.1.2. The finite element calculations were run on a VAX 8600 and each analysis took about 4.5 cpu hours. The results from the finite element method indicate reasonable agreement with the results obtained from the upper bound approach.

Figure 23a shows the deformed grid after a partial extrusion has occurred which is obtained from the finite element analysis for a die angle $\alpha = 50°$. The formation of piping defect is very obvious on expanded scale as seen in Figure 23b.

Figure 24a and 24b shows the piping defect for a die angle $\alpha = 60°$. The difference between Figure 23 and 24 is the conical die angle. The increase in the conical die angle causes an increase in the size of the pipe. This was also observed in the upper bound analysis. Therefore, the finite element analysis shows a correlation with the upper bound approach.

Figure 25 shows a comparison of the relative pipe size as determined both by the finite element method and by the upper bound approach. The relative pipe sizes calculated

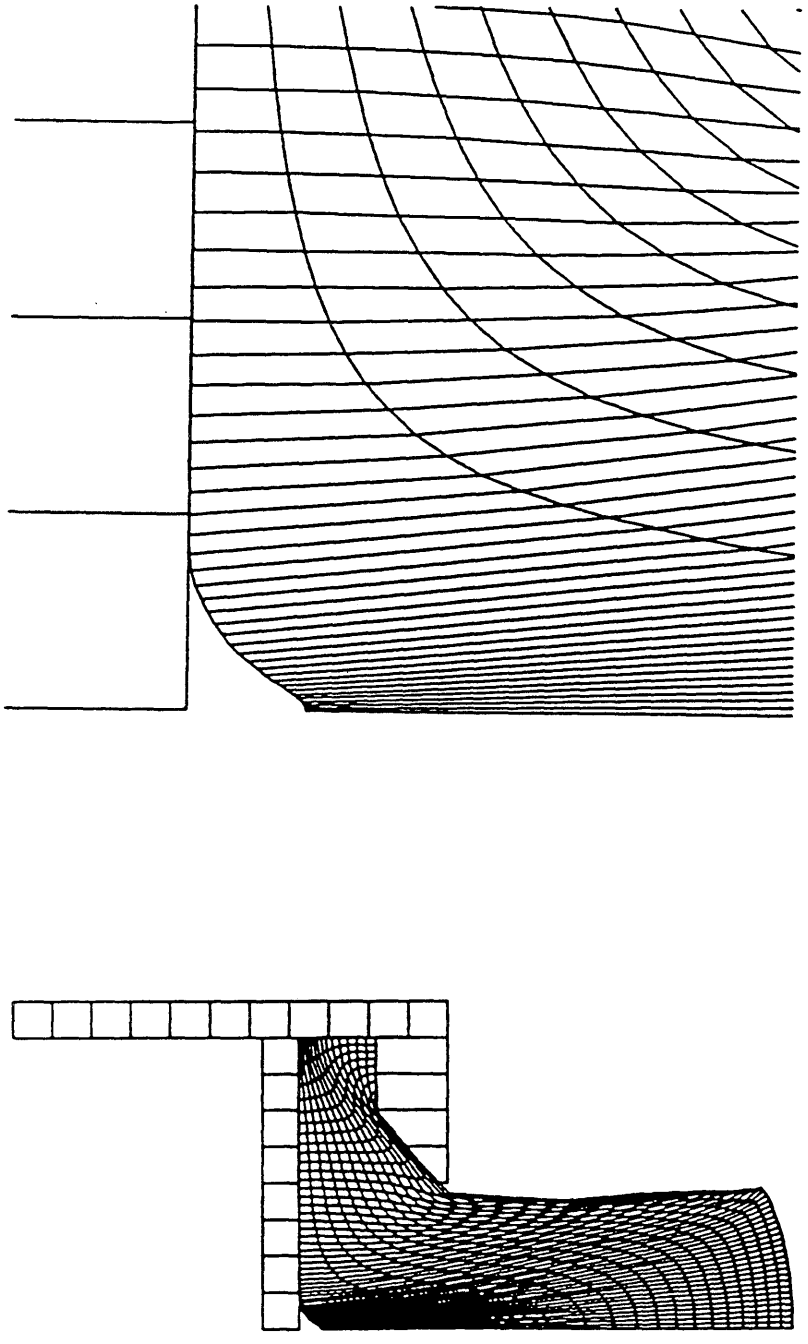

(b)

(a)

Figure 23 The formation of piping defect for $\alpha=50^{\circ}$ using NIKE2D,
(a) Full view, and
(b) an expanded scale.

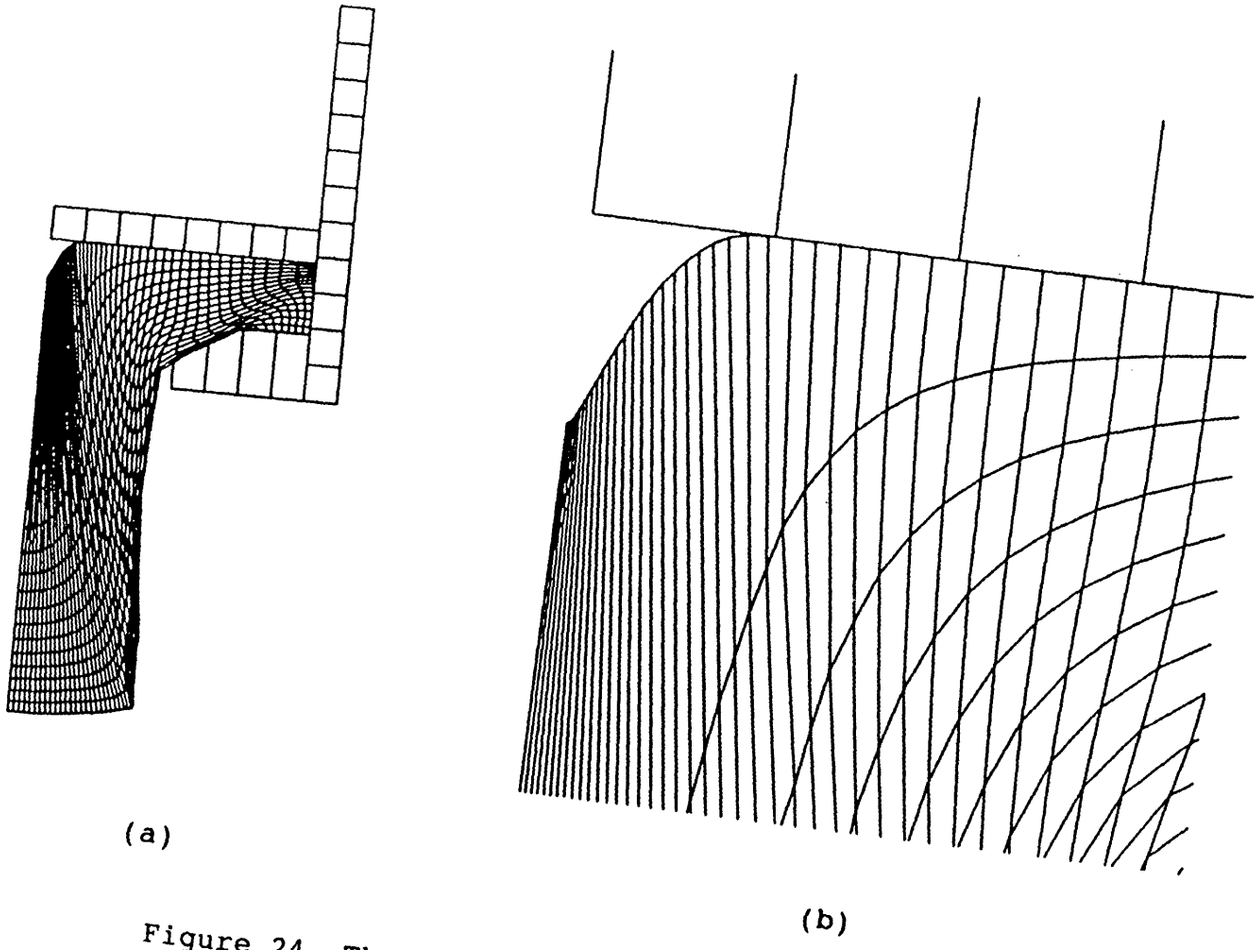

Figure 24 The formation of piping defect for $\alpha=60°$ using NIKE2D,
(a) Full view, and
(b) an expanded scale.

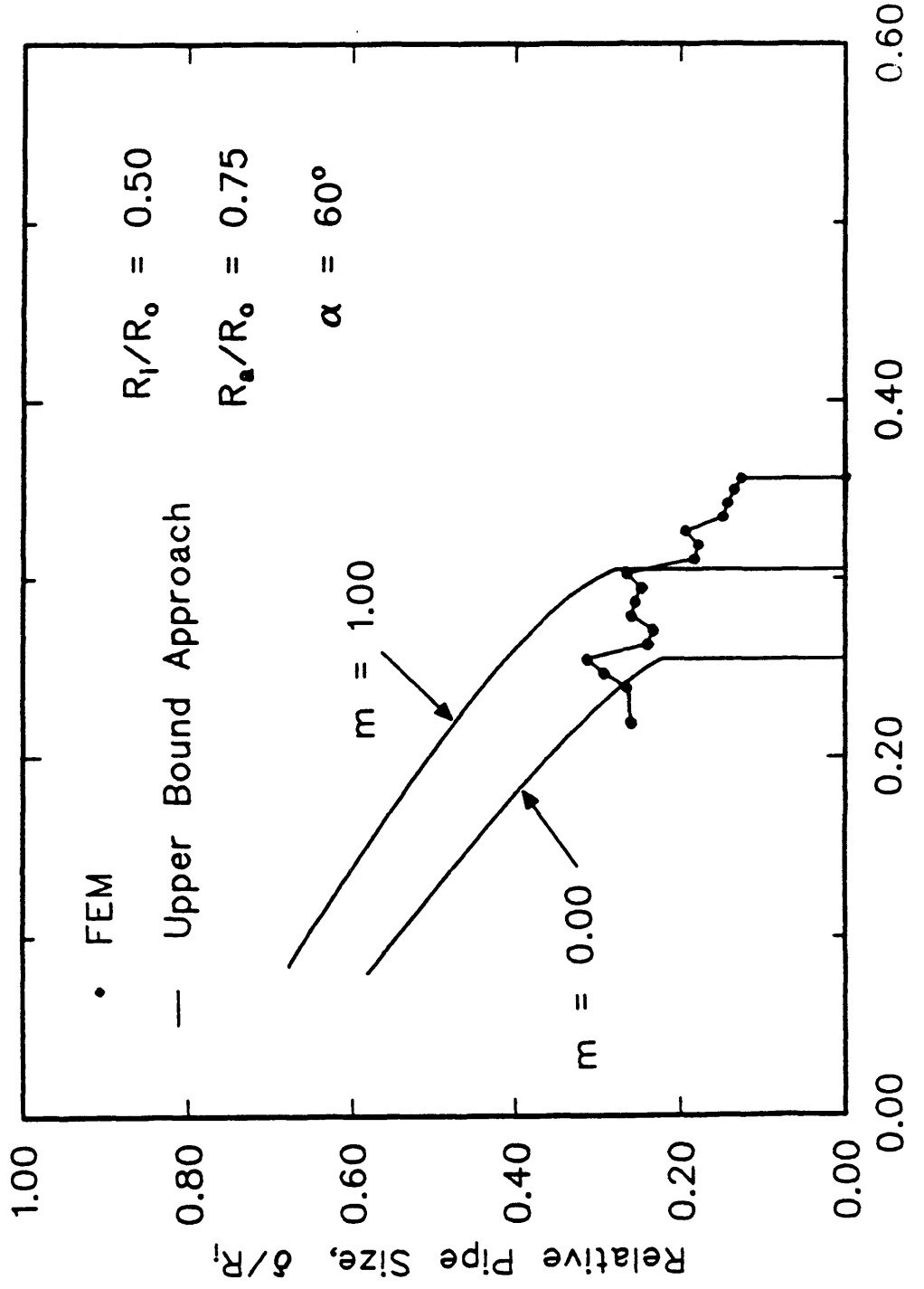

Figure 25 Comparison of relative pipe size as determined by the finite element method and the upper bound approach.

from the FEM and the upper bound approach are in reasonable agreement with each other. Both curves show a finite size for the pipe when it first occurs. The increase in the pipe size as billet length is decreased is observed in both methods. The ragged behavior of the FEM curve is due to a finite number of nodes being used to represent a continuum of material. This is inherent to the FEM.

Figure 26 shows the criteria curve for the formation of the piping defect as obtained from the upper bound analysis. This figure also shows the first appearance of a pipe as calculated by the finite element method. In order to obtain values for the finite element method, four different analysis were made, each with a different die angle. The first appearance of a pipe occurs at shorter billet lengths with decreasing conical die angle. These finite element results show the same trend as the criteria curves generated from the upper bound approach. These results provide a validation of the trends that were established from the criteria curve obtained from the upper bound approach.

There are some differences between the data obtained from the FEM and the upper bound approach. It should be noted that the use of flow patterns based upon the upper bound approach provides a method for obtaining a continuous solution which is essentially a quasi-static solution to a

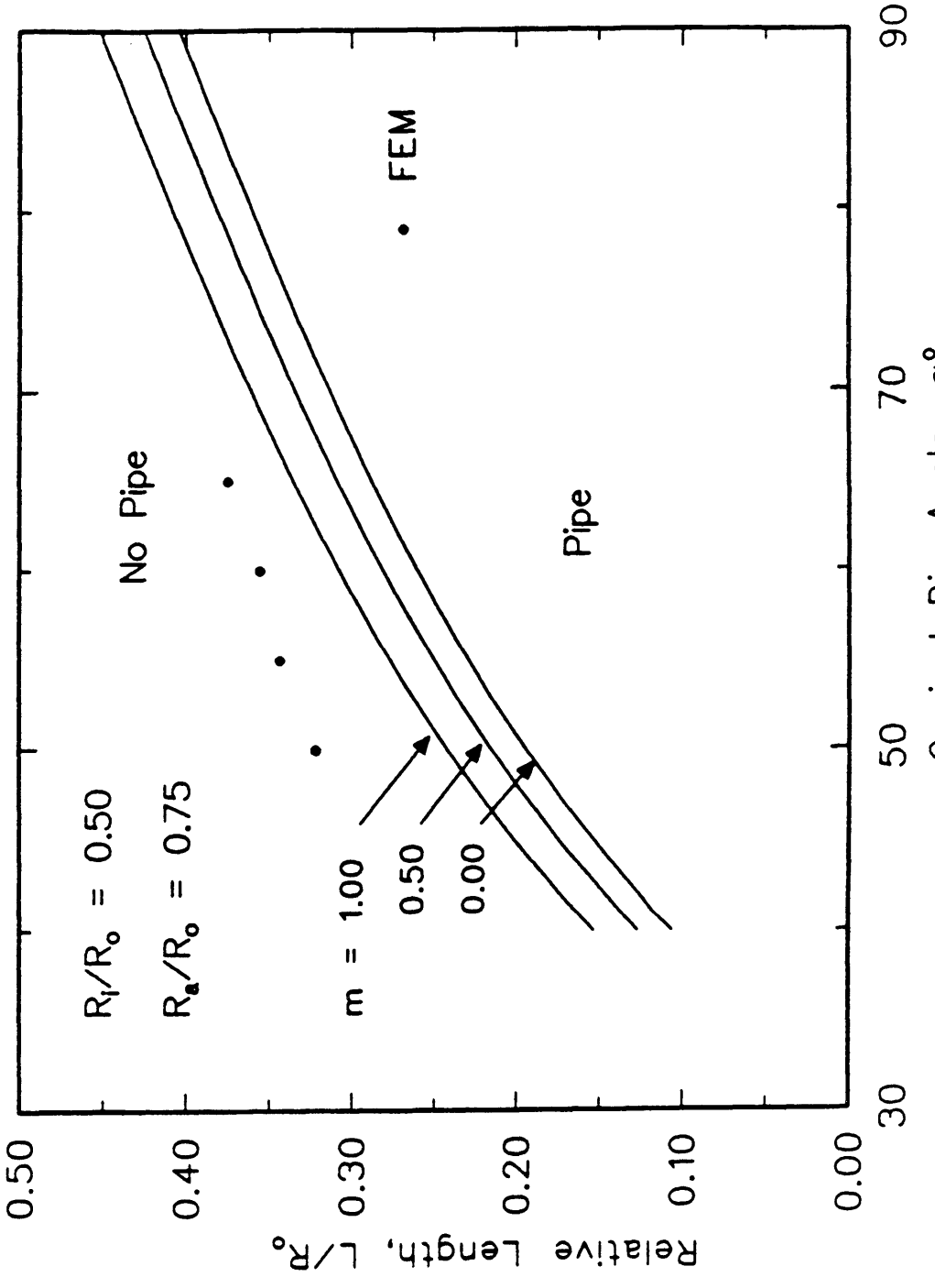

Figure 26 Comparison for occurrence of a pipe as determined by the finite element method and the upper bound approach.

metal forming problem. The finite element method is ta system which uses sets of nodes and elements in order to simulate the deformation conditions. It is an incremental process. Because of this reason, some scattered data were obtained from the finite element analysis. Nevertheless, the data shown in Figure 25 and 26 indicate that the upper bound approach and the finite element method analysis provide the same trend for the initiation and size of the piping defect.

6. CONCLUSIONS

1. An upper bound analysis for the formation of piping defect has been developed.
2. The analysis for the formation of the piping defect by the upper bound method provides a prediction for the process conditions which induce defect formation.
3. The potential for the piping defect increases with the following changes in the process parameters:

   decreasing the relative length of the non extruded portion of the billet, L/R_o

   increasing the die angle, α

   increasing the inverse reduction ratio, R_i/R_o

   decreasing the relative radius of the conical region of the die, R_a/R_o

   increasing friction factor, m.
4. Friction has a small effect on the formation of a pipe but it does have a large influence on the pressure required for extrusion to occur.
5. The finite element method analysis using NIKE2D provides reasonable confirmation for the piping defect criteria determined from the upper bound approach.

REFERENCES

1. Altan, T., H. Burte, H. Gegel, A. Make, Process Modeling : Fundamentals and Applications to Metals, ASM, Metals Park, OH, 1980.

2. Boër, C.R., H. Rebelo, H. Rydstad, and G. Schröder, Process Modeling of Metal Forming and Thermomechanical Treatment, Springer-Verlag, New York, NY, 1986.

3. Avitzur, B., Metal Forming : Process and Analysis, McGraw-Hill, New York, NY, 1968.

4. Avitzur, B., Metal Forming : The Application of Limit Analysis, Mercel Dekker, New York, NY, 1980.

5. Hosford, W. F., and R.M. Caddell, Metal Forming : Mechanics and Metallurgy, Prentice-Hall, NJ, 1983.

6. Altan, T., S.I. Oh, and H.L. Gegel, Metal Forming - Fundamentals and Applications, ASM, Metals Park, OH, 1983.

7. Avitzur, B., C.J. Van Tyne, and S. Turczyn, "The Prevention of Central Bursts during Rolling", Transactions of the ASME, Journal of Engineering for Industry, Vol. 110, 1988, p. 180.

8. Gordon, W. A., and C.J. Van Tyne, "An Analysis of the Piping Defect at the End of the Stroke in Direct Extrusions", Proceedings of NAMRC-XVI, 1988, p. 132.

9. Avitzur, B., R. Wu, S. Talbert, and Y.T. Chu, "Analysis of Core Fracture in Drawing of Bimetal Rods and Wires", Transactions of the ASME, Journal of Engineering for Industry, Vol. 108, 1986, p. 133.

10. Avitzur, B., Handbook of Metal-Forming Processes, Wilay-Interscience, Bethlehem, Pennsylvania, 1983.

11. Kalpakjian, S., Manufacturing Process for Engineering Materials, Addison-Wesley, Chicago, Illinois, 1985.

12. Johnson, W., "The Plane Strain Extrusion of Short Slugs", Journal of the Mechanics and Physics of Solids, Vol. 5, 1957, p. 202.

13. Johnson, W., "An Elemntary Consideration of Some Extrusion Defects", Applied Science Research, Section A, Vol.8, 1959, p. 52.

14. Hallquist, J.O., NIKE2D - A Vectorized Implicit Finite Deformation, Finite Element Code for Analyzing the Static and Dynamic Response of 2-D Solids with Interactive Rezoning and Graphics, Lawrence Livermore National Laboratories, Dec., 1986, UCID-19677, Rev. 1.

15. Hallquist, J.O., MAZE - An Implicit Generation for DYNA 2D and NIKE2D, Lawrence Livermore National Laboratory, June, 1983, UCID-19029, Rev. 2.

16. Hallquist, J.O., and J.L., Levatin, ORION - An Interactive Color Post-Processor for Two Dimensional Finite Element Codes, Lawrence Livermore National Laboratories, August, 1985, UCID-19310, Rev. 2.

17. Owen, D.R.J. and E. Hinton, Finite Element in Plasticity: Theory and Practise, Pineridge Press Limited, Swansw, U.K., 1980.

18. Erman. E. and S.L. Semiatin, Physical Modelling of Metal Working Processes, TMS, Warrendale, PA, 1987.

19. Prager, W. and P. G. Hodge, Theory of Perfectly Plastic Solids, Wiley, New York, NY, 1951.

20. Drucker, D. C., H. J. Greenberg, and W. Prager, "The Safety Factor of an Elastic - Plastic Body in Plane Strain, Transactions of ASME, Vol. 73, 1951, p. 371.

21. Dieter, G.E., Mechanical Metallurgy, 3rd edition, McGraw-Hill, New York, NY, 1986.

22. Gordon, A.W. and C.J. Van Tyne, "Modeling the Forward Extrusion Process", Eastern Manufacturing Technology Conference, 1989, p. 163.

23. Kobayashi, S.,"A Review on the Finite-Element Method and Metal Forming Process Modeling", Journal of Applied Metalworking, Vol. 2, 1982, p. 163.

24. Lee, C.H. and S. Kobayashi, "Elastoplastic Analysis of Plane Strain and Axisymetric Flat Punch Indentation by the Finite Element Method", Introduction Journal of Mechanical Sciences, Vol. 12, 1970, p. 349.

25. McMeeking, R.M. and Rice J.R., "Finite Element Formulations for Problems of Large Elastic-Plastic Deformation", International Journal of Solids and Structures, Vol. 11, 1975, p. 601.

26. Moon, Y.H., "An Upper Bound Analysis of a Process-Induced Surface Defect in Forgings and Extrusions", Ph.D Dissertation No T-4041, Department of Metallurgical and Materials Engineering, Colorado School of Mines, Golden, CO, 1991.

27. Frater, J.L. and G.J. Petrus, "Combining Finite Element Methods and the Cockcraft and Latham Criteria to Predict Free Surface Workability of Cold Forgings", Transaction of NAMRI/SME, 1990, p. 97.

28. Frater, J.L. and B.R. Penza, "Predicting Fracture in Load Upset Forging by Finite Element Methods", Journal of Materials Shaping Technology, Vol. 7, 1989, p. 57.

29. Avitzur, B. and C.J. Van Tyne, "Ring Forming : An Upper Bound Approach--Part I : Flow Pattern and Calculation of Power", Transactions of the ASME, Journal of Engineering for Industry, Vol. 104, 1982, p. 231.

APPENDIX I - Calculation of the velocity fields and upper bound power terms for each zone

A representation of the process is given in Figures 7 and 8. The ram pushes on the back side of the billet with a velocity $\dot{U}$. The cylindrical product exits the extrusion die with a velocity v_f. Zone I is the outer portion of the billet and it is a ring element of inner radius R_1, outer radius R_o and thickness L. The left side of zone I moves to the right at a velocity $\dot{U}$. Zone IV is the product and assumed to be rigid body which moves to the right a velocity v_f. Zone III is a complex-shaped region in which both axial and radial flow are occurring. Zone II is similar to zone III. Zone I, zone II and zone III have material deformation occuring within them. The volumes of zone II, zone III and zone IV are all dependent on the die angle α and the pseudo-independent parameter (either δ or ε) whose value changes with the other process variables. The surface Γ_1 between zone I and zone II is a cylindrical surface. The surface is fixed at R_a. The surface Γ_2, which separates zone II and zone III, is also a cylindrical surface. This surface is fixed at R_i. The surface Γ_3, is assumed to be a conical surface, between zone III and zone IV but its exact position is variable, depending on the pseudo-independent parameter ε

or δ. The value that the pseudo-independent parameter possesses will be determined through the principle of minumum energy.

The velocity field in cylindirical coordinates can be expressed by the following equations.

From a material balance in zone I, the material into the control volume is

$$= \dot{U}\Delta t\pi(R_o^2 - R^2) \tag{1.1}$$

and material out of the control volume is

$$= -\dot{U}_R\Delta t\pi 2LR \tag{1.2}$$

The material into the control volume must be equal the material out of the control volume. Therefore,

$$\dot{U}_R = -\frac{\dot{U}R}{2L}\left[\left(\frac{R_o}{R}\right)^2 - 1\right] \tag{1.3}$$

For a cylindrical coordinate system (R,θ,y) the strain rates can be calculated from the velocity field via the

following equations (8).

$$
\begin{aligned}
\dot{\varepsilon}_{RR} &= \frac{\partial \dot{U}_R}{\partial R} \\
\dot{\varepsilon}_{\theta\theta} &= \frac{1}{R}\frac{\partial \dot{U}_\theta}{\partial \theta} + \frac{\dot{U}_R}{R} \\
\dot{\varepsilon}_{yy} &= \frac{\partial \dot{U}_y}{\partial y} \\
\dot{\varepsilon}_{R\theta} &= \frac{1}{2}\left[\frac{\partial \dot{U}_\theta}{\partial R} - \frac{\dot{U}_\theta}{R} + \frac{1}{R}\frac{\partial \dot{U}_R}{\partial \theta}\right] \\
\dot{\varepsilon}_{\theta y} &= \frac{1}{2}\left[\frac{\partial \dot{U}_\theta}{\partial y} + \frac{1}{R}\frac{\partial \dot{U}_y}{\partial \theta}\right] \\
\dot{\varepsilon}_{yR} &= \frac{1}{2}\left[\frac{\partial \dot{U}_R}{\partial y} + \frac{\partial \dot{U}_y}{\partial R}\right]
\end{aligned}
\qquad (1.4)
$$

The law of incompressibility requires that the sum of the principal srain rates must be zero. Mathematically,

$$\dot{\varepsilon}_{RR} + \dot{\varepsilon}_{\theta\theta} + \dot{\varepsilon}_{yy} = 0 \qquad (1.5)$$

Therefore, the strain rates for zone I are

$$\dot{\varepsilon}_{RR} = \frac{\dot{U}}{2L}\left[\left(\frac{R_o}{R}\right)^2 + 1\right]$$

$$\dot{\varepsilon}_{\theta\theta} = -\frac{\dot{U}}{2L}\left[\left(\frac{R_o}{R}\right)^2 - 1\right] \qquad (1.6)$$

$$\dot{\varepsilon}_{YY} = -\frac{\dot{U}}{L}$$

$$\dot{\varepsilon}_{R\theta} = \dot{\varepsilon}_{\theta Y} = \dot{\varepsilon}_{YR} = 0$$

If $\dot{\varepsilon}_{RR}$ is integreted the axial velocity can be obtained

$$\dot{U}_y - \dot{U}_y\big|_{y=0} = \int_0^y \dot{\varepsilon}_{RR}\, dy \qquad (1.7)$$

$$\dot{U}_y = \dot{U}\left(1 - \frac{Y}{L}\right)$$

In summary, the velocity assumed for zone I is:

$$\dot{U}_R = -\frac{\dot{U}R}{2L}\left[\left(\frac{R_o}{R}\right)^2 - 1\right]$$
$$\dot{U}_y = \dot{U}\left(1 - \frac{y}{L}\right) \qquad (1.8)$$
$$\dot{U}_\theta = 0$$

From a material balance on zone II, the material into the control volume is

$$= -\dot{U}_R 2\pi R_a \Delta t + \dot{U}\Delta t \pi (R_a - R^2) \qquad (1.9)$$

and the material out of the control volume is

$$= -\dot{U}_R W 2\pi R \Delta t \qquad (1.10)$$

where

$$\frac{W}{R_i} = \left(\frac{L}{R_o}\frac{R_o}{R_i}\right) + \cot\alpha\left(\frac{R_a}{R_i} - \frac{R}{R_i}\right) \tag{1.11}$$

In Eq. (1.11), W(R) is the equation for the interface surface between the die and zone II. The velocity field for zone II is

$$\begin{aligned} \dot{U}_R &= -\frac{\dot{U}R}{2W}\left[\left(\frac{R_o}{R}\right)^2 - 1\right] \\ \dot{U}_y &= \dot{U}\left[1 - \frac{y}{W}\left[1 + \frac{R}{2W}\frac{\partial W}{\partial R}\left(\left(\frac{R_o}{R}\right)^2 - 1\right)\right]\right] \\ \dot{U}_\theta &= 0 \end{aligned} \tag{1.12}$$

For zone IV, the material into the zone is

$$= \dot{U}\Delta t\,\pi\left(R_o^2 - \delta^2\right) \tag{1.13}$$

and material out of the zone is

$$= v_f \Delta t \pi (R_i^2 - \delta^2) \tag{1.14}$$

The pseudo-independent variable δ is used in these equations. Equavalent equation using ε can be obtained by either derivation or by substitution of the proper ε-δ relationship (see Eq. (10) in the main body of the text). Thus, the velocity field for zone IV is:

$$\dot{U}_R = 0$$

$$\dot{U}_y = v_f = \frac{\dot{U}\left[\left(\frac{R_o}{R}\right)^2 - \left(\frac{\delta}{R_i}\right)^2\right]}{1 - \left(\frac{\delta}{R_i}\right)^2} \tag{1.15}$$

$$\dot{U}_\theta = 0$$

In zone III, a material balance yields

$$\dot{U}_R(L + L_a)\, 2\pi R_i \Delta t + \pi(R_i - R^2) = v_f \Delta t \pi (R_i^2 - R^2) - \dot{U}_R Z\, 2\pi R \Delta t \tag{1.16}$$

where

$$\frac{Z}{R_i} = \left(\frac{L}{R_o}\frac{R_o}{R_i} - \frac{\varepsilon}{R_i}\right)\frac{R}{R_i} + \frac{\varepsilon}{R_i} \tag{1.17}$$

In equation (1.17), Z(R) is the equation for the surface between zone III and zone IV (i.e. it is the equation for Γ_2).

Hence, the velocity field in zone III is:

$$\begin{aligned}
\dot{U}_R &= -\frac{\dot{U}R}{2Z}\left[1 - \left(\frac{\delta}{R}\right)^2\right]\left[\frac{\left(\frac{R_o}{R_i}\right) - 1}{1 - \left(\frac{\delta}{R}\right)^2}\right] \\
\dot{U}_Y &= \dot{U}\left[1 + \frac{Y}{Z}\left(1 - \frac{R}{2Z}\frac{\partial Z}{\partial R}\left(1 - \left(\frac{\delta}{R}\right)^2\right)\frac{\left(\frac{R_o}{R_i}\right)^2 - 1}{1 - \left(\frac{\delta}{R_i}\right)^2}\right)\right] \\
\dot{U}_\theta &= 0
\end{aligned} \tag{1.18}$$

By the upper bound approach, the internal power of the deformation is given by

$$\dot{W}_i = \int_V \frac{2\sigma_o}{\sqrt{3}} \sqrt{\frac{1}{2}\dot{\varepsilon}_{ij}\dot{\varepsilon}_{ij}}\ dV \tag{1.19}$$

where V is the volume of the material and the $\dot{\varepsilon}_{ij}$'s are the strain rates.

The internal power of deformation for zone I is

$$\begin{aligned}\dot{W}_{i_I} &= \int_V \frac{2\sigma_o}{\sqrt{3}} \sqrt{\frac{1}{2}\dot{\varepsilon}_{RR}^2 + \frac{1}{2}\dot{\varepsilon}_{\theta\theta}^2 + \frac{1}{2}\dot{\varepsilon}_{yy}^2 + \dot{\varepsilon}_{R\theta}^2 + \dot{\varepsilon}_{y\theta}^2 + \dot{\varepsilon}_{yR}^2}\ dV \\ &= \int_{R_a}^{R_o}\int_0^L\int_0^{2\pi} \frac{2\sigma_o}{\sqrt{3}} \left[\frac{1}{2}\left[\frac{\dot{U}}{2L}\left(\left(\frac{R_o}{R}\right)^2 + 1\right)\right]^2\right. \\ &\quad \left. + \frac{1}{2}\left[\left[-\frac{\dot{U}}{2L}\left(\left(\frac{R_o}{R}\right)^2 - 1\right)\right]^2 + \frac{1}{2}\left(-\frac{\dot{U}}{L}\right)^2\right]\right]^{1/2} R\,d\theta\,dy\,dR\end{aligned} \tag{1.20}$$

where

$$dV = Rd\theta dydR \tag{1.21}$$

Integration yields,

$$\dot{W}_{i_I} = \frac{\sigma_o \pi \dot{U}}{\sqrt{3}} R_o^2 \left[2 - \sqrt{3\left(\frac{R_a}{R_o}\right)^4 + 1} + \ln\left(\left(\frac{R_o}{R_a}\right)^2 \frac{1 + \sqrt{3\left(\frac{R_a}{R_o}\right)^4 + 1}}{3} \right) \right] \tag{1.22}$$

For zone II, the internal power of deformation is

$$\dot{W}_{i_{II}} = \int_{R_i}^{R_a}\int_0^W\int_0^{2\pi} \frac{2\sigma_o}{\sqrt{3}}\left[\frac{1}{2}\left[\frac{\dot{U}}{2\dot{W}}\left(\left(\frac{R_o}{R}\right)^2 + 1\right) + \frac{R}{\dot{W}}\frac{\partial \dot{W}}{\partial R}\left(\left(\frac{R_o}{R}\right)^2 - 1\right)\right]^2\right.$$
$$+ \frac{1}{2}\left[-\frac{\dot{U}}{2\dot{W}}\left(\left(\frac{R_o}{R}\right)^2 - 1\right)\right]^2 + \frac{1}{2}\left[-\frac{\dot{U}}{Z}\left(1 + \frac{1}{2}\frac{R}{\dot{W}}\frac{\partial \dot{W}}{\partial R}\left(\left(\frac{R_o}{R}\right)^2 - 1\right)\right)\right]^2 \qquad (1.23)$$
$$+ \left[\frac{1}{4}\frac{\dot{U}y}{W^2}\left[\left(3 + \left(\frac{R_o}{R}\right)^2\right)\frac{\partial W}{\partial R} + \frac{2R}{W}\left(\left(\frac{R_o}{R}\right)^2 - 1\right)\left(\frac{\partial W}{\partial R}\right)^2\right.\right.$$
$$\left.\left.\left. - R\left(\left(\frac{R_o}{R}\right)^2 - 1\right)\frac{\partial^2 W}{\partial R^2}\right]\right]^2\Bigg]^{1/2} R\,d\theta\,dy\,dR$$

Integration yields,

$$\dot{W}_{i_{II}} = \frac{\sigma_o}{\sqrt{3}}\pi\dot{U}R_o^2\int_1^{R_a/R_i}\frac{p}{2}\left[\sqrt{1+B} + B\ln\left(1 + \frac{\sqrt{1+B}}{\sqrt{B}}\right)\right]\rho\,d\rho \qquad (1.24)$$

where

$$B = \frac{(f + 2 + \gamma)^2 + f^2 + (2 + \gamma)^2}{p^2/2} \tag{1.25}$$

and

$$p = 2\gamma V_{II} + (f + 4) V_{II} - f\rho \frac{\partial V_{II}}{\partial \rho} \tag{1.26}$$

with

$$\begin{aligned} \rho &= \frac{R}{R_i} \\ V_{II} &= \frac{\partial W}{\partial R} \\ f &= \left(\frac{R_o}{R_i}\right)^2 \frac{1}{\rho} - 1 \\ \gamma &= \rho f V_{II} \frac{R_i}{W} \end{aligned} \tag{1.27}$$

For zone III,

$$W_{i_{III}} = \int_{\delta}^{R_i}\int_{0}^{Z}\int_{0}^{2\pi} \frac{2\sigma_o}{\sqrt{3}}\left[\frac{(\frac{R_o}{R_i})^2 - 1}{1 - (\frac{\delta}{R_i})^2}\right]\left[\frac{1}{2}\left[-\frac{\dot{U}}{2Z}\left((\frac{\delta}{R})^2 + 1 - \frac{R}{Z}\frac{\partial Z}{\partial R}\left(1-(\frac{\delta}{R})^2\right)\right)\right]^2 + \frac{1}{2}\left[-\frac{\dot{U}}{2Z}\left(1 - (\frac{\delta}{R})^2\right)\right]^2 + \frac{1}{2}\left[\frac{\dot{U}}{Z}\left[1 - \frac{1}{2}\frac{R}{Z}\frac{\partial Z}{\partial R}\left(1 - (\frac{\delta}{R})^2\right)\right]\right]^2 + \left[-\frac{\dot{U}y}{4Z^2}\left(\left(3 + (\frac{\delta}{R})^2\right)\frac{\partial Z}{\partial R} - \frac{2R}{z}\left(1 - (\frac{\delta}{R})^2\right)(\frac{\partial Z}{\partial R})^2 + R\left(1 - (\frac{\delta}{R})^2\right)\frac{\partial^2 Z}{\partial R^2}\right)\right]^2\right]^{1/2} Rd\theta dydR \tag{1.28}$$

The internal power of deformation for zone III is

$$\dot{W}_{i_{III}} = \frac{\sigma_o}{\sqrt{3}}\pi\dot{U}R_o(\frac{R_i}{R_o})\left[\frac{(\frac{R_o}{R_i}) - 1}{1 - (\frac{\delta}{R_i})^2}\right] \cdot \int_{\delta/R_i}^{1} \frac{q}{2}\left[\sqrt{1 + A} + A\ln\left(1 + \frac{\sqrt{1 + A}}{A}\right)\right]\rho d\rho \tag{1.29}$$

where

$$A = \frac{(2 - e - \beta)^2 + e^2 + (2 - \beta)^2}{q^2/2} \tag{1.30}$$

and

$$q = -2V_{III}\beta + (4 - e)V_{III} + e\rho\frac{\partial V_{III}}{\partial \rho} \tag{1.31}$$

with

$$\begin{aligned} \rho &= \frac{R}{R_i} \\ V_{III} &= \frac{\partial Z}{\partial R} \\ e &= 1 - \frac{1}{\rho^2}\left(\frac{\delta}{R_i}\right)^2 \\ \beta &= \rho e V_{III}\frac{R_i}{Z} \end{aligned} \tag{1.32}$$

Zone IV is assumed to move as a rigid body, therefore there is no internal deformation in this zone.

There are internal shear losses along the surfaces of velocity discontinuity. These losses can be calculated by

$$\dot{W}_s = \int_{s_\Gamma} \frac{\sigma_o}{\sqrt{3}} |\Delta v| \, dS \tag{1.33}$$

where S is the surface between the two regions and Δv is the tangential velocity difference that exists along the surfaces.

For the surface Γ_1, between zone I and zone II, the velocity discontinuity is

$$|\Delta v| = \left| \dot{U}\left(1 - \frac{Y}{L}\right) - \dot{U}\left[1 - \frac{Y}{\bar{W}}\left[1 + \frac{R_a}{2\bar{W}} \frac{\partial \bar{W}}{\partial R}\left(\left(\frac{R_o}{R_a}\right)^2 - 1\right)\right]\right] \right| \tag{1.34}$$

therefore, the shear power losses along surface Γ_1 are

$$\dot{W}_{S_{\Gamma_1}} = \int_0^L \int_0^{2\pi} \frac{\sigma_o}{\sqrt{3}} \left| \dot{U}\left(1 - \frac{Y}{L}\right) - \dot{U}\left[1 - \left(\frac{Y}{W}\right) + \left(1 + \frac{R_a}{2W}\right)\frac{\partial W}{\partial R}\left(\left(\frac{R_o}{R_a}\right)^2 - 1\right)\right]\right| R_a d\theta dy \tag{1.35}$$

where

$$dS = R_a d\theta dy \tag{1.36}$$

Integration yields,

$$\dot{W}_{S_{\Gamma_1}} = \frac{\pi\sigma_o \dot{U}}{\sqrt{3}} \frac{1}{2} R_o^2 \left(\frac{R_a}{R_o}\right)^2 \cot\alpha \left[\left(\frac{R_o}{R_a}\right)^2 - 1\right] \tag{1.37}$$

For the surface Γ_2, between zone II and zone III, the velocity discontinuity is

$$|\Delta v| = \left| \dot{U}\left[1 + \frac{Y}{Z}\left[1 - \frac{R_i}{2Z}\frac{\partial Z}{\partial R}\left(1 - \left(\frac{\delta}{R_i}\right)^2\right)\right]\frac{\left(\frac{R_o}{R_i}\right)^2 - 1}{1 - \left(\frac{\delta}{R_i}\right)^2}\right] \right. \tag{1.38}$$
$$\left. -\dot{U}\left[1 - \frac{Y}{Z}\left[1 + \frac{R_i}{2Z}\frac{\partial Z}{\partial R}\left(\left(\frac{R_o}{R_i}\right)^2 - 1\right)\right]\right]\right|$$

therefore,

$$\dot{W}_{s_{\Gamma_2}} = \int_0^Z \int_0^{2\pi} \frac{\sigma_o}{\sqrt{3}} \left| \dot{U}\left[\left[1 + \frac{Y}{Z}\left(1 - \frac{R_i}{2Z}\frac{\partial Z}{\partial R}\left(1 - \left(\frac{\delta}{R_i}\right)^2\right)\right)\frac{\left(\frac{R_o}{R_i}\right)^2 - 1}{1 - \left(\frac{\delta}{R_i}\right)^2}\right]\right.\right. \tag{1.39}$$
$$\left.\left. -\dot{U}\left[1 - \frac{Y}{Z}\left(1 + \frac{R_i}{2Z}\frac{\partial Z}{\partial R}\left(\left(\frac{R_o}{R_i}\right)^2 - 1\right)\right)\right]\right] \right| R_i d\theta dy$$

where

$$dS = R_i \, d\theta \, dy \tag{1.40}$$

Integration yields,

$$\dot{W}_{S_{\Gamma_2}} = \frac{\pi\sigma_o}{\sqrt{3}} R_o^2 \left[\left(\frac{R_o}{R_i}\right)^2 - 1 \right] \left[\left(\frac{L}{R_i}\right) + \left(\frac{R_a}{R_i} - 1\right)\cot\alpha \left(\frac{1}{\left(\frac{R_o}{R_i}\right)^2 - 1} + \frac{1}{1 - \left(\frac{\delta}{R_i}\right)^2} \right) + \frac{1}{2}\left(-\cot\alpha - V_{III}\big|_{R_i}\right) \right] \tag{1.41}$$

where

$$V_{III}\big|_{R_i} = \frac{L + (R_a - R_i)\cot\alpha}{(R_i - \delta)} \tag{1.42}$$

For the surface Γ_3, between zone III and zone IV, the velocity discontinuity is

$$|\Delta v| = |\dot{U}_{y_{IV}} \sin\phi - \dot{U}_{y_{III}} \sin\phi - \dot{U}_{R_{III}} \cos\phi| \tag{1.43}$$

where ϕ is the angle of the Γ_3 surface.

The shear power losses along the surface Γ_3 are

$$\dot{W}_{S_{\Gamma_3}} = \int_{\delta}^{R_i}\int_{0}^{2\pi}\frac{\sigma_o}{\sqrt{3}}\left|\dot{U}\frac{(\frac{R_o}{R_i})^2 - (\frac{\delta}{R_i})^2}{1 - (\frac{\delta}{R_i})^2}\frac{V_{III}}{\sqrt{1 + V_{III}^2}}\right.$$

$$- \dot{U}\left[1 + \frac{Z}{y}\left(1 - \frac{R}{2Z}V_{III}\left(1-(\frac{\delta}{R})^2\right)\frac{(\frac{R_o}{R_i})^2 - (\frac{\delta}{R_i})^2}{1 - (\frac{\delta}{R_i})^2}\right)\frac{V_{III}}{\sqrt{1 + V_{III}^2}}\right] \quad (1.44)$$

$$\left. + \dot{U}\left[\frac{R}{2Z}\left(1 - (\frac{\delta}{R})^2\right)\frac{(\frac{R_o}{R_i})^2 - 1}{1 - (\frac{\delta}{R_i})^2}\frac{1}{\sqrt{1 + V_{III}^2}}\right]\right| R d\theta dR$$

Integration yields,

$$\dot{W}_{S_{\Gamma_3}} = \int_{\delta}^{R_i}\int_{0}^{2\pi}\frac{\sigma_o}{\sqrt{3}}\left|\dot{U}\frac{(\frac{R_o}{R_i})^2 - (\frac{\delta}{R_i})^2}{1 - (\frac{\delta}{R_i})^2}\frac{V_{III}}{\sqrt{1 + V_{III}^2}}\right.$$

$$- \dot{U}\left[1 + \frac{Z}{y}\left(1 - \frac{R}{2Z}V_{III}\left(1-(\frac{\delta}{R})^2\right)\frac{(\frac{R_o}{R_i})^2 - (\frac{\delta}{R_i})^2}{1 - (\frac{\delta}{R_i})^2}\right)\frac{V_{III}}{\sqrt{1 + V_{III}^2}}\right] \quad (1.45)$$

$$\left. + \dot{U}\left[\frac{R}{2Z}\left(1 - (\frac{\delta}{R})^2\right)\frac{(\frac{R_o}{R_i})^2 - 1}{1 - (\frac{\delta}{R_i})^2}\frac{1}{\sqrt{1 + V_{III}^2}}\right]\right| \sqrt{1 + V_{ii}^2}\, R dR$$

where

$$V_{III} = \frac{\partial Z}{\partial R} = \frac{\frac{L'}{R} + (\frac{R_a}{R} - 1)\cot\alpha}{1 - \frac{\delta}{R}} \qquad (1.46)$$

$$dS = \sqrt{1 + V_{III}^2}\, R dR$$

The friction losses along workpiece/tool interface can be determined by

$$\dot{W}_f = \int_S \frac{m\sigma_o}{\sqrt{3}} |\Delta v|\, dS \qquad (1.47)$$

where m is the constant friction factor and Δv is tangential velocity differences between the tool and the workpiece at the interface and S is the interfacial surface.

The velocity difference between zone II and the die is

$$\Delta v = \left| \frac{\dot{U}_{R_{II}}}{\sin\alpha} \Big|_{y=W} - 0 \right| = \left| \dot{U} \frac{R}{2W} \left[\left(\frac{R_o}{R} \right)^2 - 1 \right] \right| \frac{1}{\sin\alpha} \tag{1.48}$$

The frictional power losses along surface S_a are

$$\dot{W}_{f_a} = \int_0^{2\pi} \int_{R_i}^{R_a} \frac{m\sigma_o}{\sqrt{3}} \frac{\dot{U}}{2\sin\alpha} \frac{1}{\sin\alpha} \cdot \left| \frac{R}{L + R_a\cot\alpha - R\cot\alpha} \left[\left(\frac{R_o}{R} \right)^2 - 1 \right] \right| R d\theta dR \tag{1.49}$$

where

$$dS = \frac{1}{\sin\alpha} R d\theta dR \tag{1.50}$$

Integration yields,

$$\dot{W}_{f_a} = \frac{m\sigma_o}{\sqrt{3}} \frac{\pi \dot{U} R_o^2}{\sin\alpha\cos\alpha} \left[\left[1 - \left(\frac{L/R_o}{\cot\alpha} + \frac{R_a}{R_o} \right)^2 \right] \cdot \ln \left(\frac{\frac{L/R_o}{\cot\alpha} + \frac{R_a}{R_o} - \frac{R_i}{R_o}}{\frac{L/R_o}{\cot\alpha}} \right) + \frac{1}{2} \left(\frac{L/R_o}{\cot\alpha} \right)^2 - \frac{1}{2} \left(\frac{L/R_o}{\cot\alpha} + \frac{R_a}{R_o} - \frac{R_i}{R_o} \right)^2 + 2 \left(\frac{L/R_o}{\cot\alpha} + \frac{R_a}{R_o} \right) \left(\frac{R_a}{R_o} - \frac{R_i}{R_o} \right) \right] \tag{1.51}$$

The velocity difference between zone I and the die is

$$|\Delta v| = \left| -\frac{\dot{U}R}{2L}\left[\left(\frac{R_o}{R}\right)^2 - 1\right] - 0 \right| \tag{1.52}$$

The frictional power losses along surface S_b are

$$\dot{W}_{f_b} = \int_{R_a}^{R_o}\int_0^{2\pi} \frac{m\sigma_o}{\sqrt{3}} \left| -\dot{U}\frac{R}{\sqrt{3}}\left[\left(\frac{R_o}{R}\right)^2 - 1\right]\right| Rd\theta dR \tag{1.53}$$

where

$$dS = Rd\theta dR \tag{1.54}$$

Integration yields,

$$\dot{W}_{f_b} = \frac{m\sigma_o \pi}{\sqrt{3}} \dot{U} R_o^2 \left(\frac{R_o}{L}\right)\left[\frac{2}{3} - \frac{R_a}{R_o} + \frac{1}{3}\left(\frac{R_a}{R_o}\right)^3\right] \tag{1.55}$$

The velocity difference between zone I and the chamber is

$$|\Delta v| = \left|\dot{U}\left(1 - \frac{y}{L}\right) - 0\right| \tag{1.56}$$

The frictional power losses along surface S_c are

$$\dot{W}_{f_c} = \int_0^L \int_0^{2\pi} \frac{m\sigma_o}{\sqrt{3}} \left|\dot{U}\left(1 - \frac{y}{L}\right)\right| R_o d\theta dy \tag{1.57}$$

where

$$dS = R_o d\theta dy \tag{1.58}$$

Integration yields,

$$\dot{W}_{f_c} = \frac{m\sigma_o}{\sqrt{3}}\pi\dot{U}R_o^2\left(\frac{L}{R_o}\right) \tag{1.59}$$

The frictional power losses along S_d, which is between zone I and the ram, are equal to the frictional power losses along surface S_b. Therefore,

$$\dot{W}_{f_d} = \frac{m\sigma_o}{\sqrt{3}}\pi\dot{U}R_o^2\left(\frac{L}{R_o}\right) \tag{1.60}$$

The velocity difference between zone II and the ram is

$$|\Delta v| = \left|\dot{U} - \frac{R}{2\dot{W}}\left[\left(\frac{R_o}{R}\right)^2 - 1\right] - 0\right| \tag{1.61}$$

The frictional power losses along surface S_e are

$$\dot{W}_{f_e} = \int_{R_i}^{R_a}\int_0^{2\pi}\frac{m\sigma_o}{\sqrt{3}}\left|\dot{U} - \frac{R}{2\dot{W}}\left[\left(\frac{R_o}{R}\right)^2 - 1\right]\right| Rd\theta dR \tag{1.62}$$

where

$$dS = Rd\theta dR \tag{1.63}$$

Integration yields,

$$\dot{W}_{f_e} = \frac{m\sigma_o\pi}{\sqrt{3}}\dot{U}R_o^2\tan\alpha\left[\left(1 - \left(\frac{L}{R_o}\tan\alpha + \frac{R_a}{R_o}\right)\right)\right.$$
$$\cdot \ln\left[\frac{\frac{L}{R_o}\tan\alpha + \left(\frac{R_a}{R_o} - \frac{R_i}{R_o}\right)}{\frac{L}{R_o}\tan\alpha}\right] + 3\frac{L}{R_o}\tan\alpha\left(\frac{R_a}{R_o} - \frac{R_i}{R_o}\right) \tag{1.64}$$
$$\left. + \frac{1}{2}\left(\frac{R_a}{R_o} - \frac{R_i}{R_o}\right)^2 + 2\frac{R_a}{R_o}\left(\frac{R_a}{R_o} - \frac{R_i}{R_o}\right)\right]$$

The velocity difference between zone III and the ram is

$$|\Delta v| = \left| -\dot{U}\frac{R}{2\bar{Z}}\left[1 - \left(\frac{\delta}{R}\right)^2\right]\left[\frac{\left(\frac{R_o}{R_i}\right)^2}{1 - \left(\frac{\delta}{R_i}\right)^2}\right] - 0\right| \tag{1.65}$$

The frictional power losses along surface S_f are

$$\dot{W}_{f_f} = \int_{\delta}^{R_i} \int_{0}^{2\pi} \frac{m\sigma_o}{\sqrt{3}} \left| -\dot{U}\frac{R}{2Z}\left[1 - \left(\frac{\delta}{R}\right)^2\right]\left[\frac{\left(\frac{R_o}{R_i}\right)^2 - 1}{1 - \left(\frac{\delta}{R_i}\right)}\right] \right| Rd\theta dR \qquad (1.66)$$

where

$$dS = Rd\theta dR \qquad (1.67)$$

Integration yields,

$$\dot{W}_{f_f} = m\frac{\sigma_o}{\sqrt{3}}\pi\dot{U}R_o^2\left(\frac{R_i}{R_o}\right)^3\frac{1}{2}\frac{\left[\left(\frac{R_o}{R_i}\right)^2 - 1\right]}{\left[1 - \left(\frac{\delta}{R_i}\right)^2\right]}\frac{\left[\left(1 - \frac{\delta}{R_i}\right)^2\left(1 + 3\frac{\delta}{R_i}\right)\right]}{\left[\frac{L}{R_o} + \left(\frac{R_a}{R_o} - \frac{R_i}{R_o}\right)\cot\alpha\right]} \qquad (1.68)$$

By summing all the power losses and the internal power of deformation terms, the upper bound on the power can be determined as

$$J^* = \dot{W}_{i_I} + \dot{W}_{i_{II}} + \dot{W}_{i_{III}} + \dot{W}_{s_{\Gamma_1}} + \dot{W}_{s_{\Gamma_2}} + \dot{W}_{s_{\Gamma_3}} + \dot{W}_{f_a} + \dot{W}_{f_b} + \dot{W}_{f_c} + \dot{W}_{f_d} + \dot{W}_{f_e} + \dot{W}_{f_f} \tag{1.69}$$

Instead of analyzing how J^* changes with variations in the process parameters, it is more meaningful to relate J^* to the ram pressure and examine how the ram pressure is affected by each of the process variables. The power consumed in the process is transmitted through the ram. Mathematically,

$$J^* = \dot{U}\pi p_{AVE} R_o^2 \tag{1.70}$$

where p_{AVE} is the average ram pressure.

By equating the above equation to the sum of the internal powers of deformation, internal shear power losses and frictional power losses, the relative average ram pressure can be determined. This would be

$$\frac{p_{AVE}}{\sigma_o} = \frac{J^*}{\dot{U}\pi R_o^2} \qquad (1.71)$$

$$\frac{p_{AVE}}{\sigma_o} = \left(\frac{R_o}{R_i}, \frac{L}{R_o}, \frac{R_a}{R_o}, \alpha, m \;\&\; \frac{\delta}{R_i}\right)$$

According to this function form, the pressure is determined as a function of the geometry, the friction constant m and the pseudo-independent parameter, δ.